



KTH Royal Institute of Technology
STOCKHOLM 2018

Fatigue life prediction of steel bridges using a small scale monitoring system

John Leander

Department of Civil and Architectural Engineering
Division of Structural Engineering and Bridges

Summary

With an increasing number of bridges approaching their expected service life, improved and new methods for accurate assessment methods are called for. Economical restraints and sustainability reasons will not allow bridge managers to replace the numerous bridges that theoretically will be judged unsafe. As a method for refined assessment, in-service monitoring can be used to accurately determine the actual structural response. This will enable an alleviation of conservative estimates and facilitate accurate service life predictions.

For fatigue assessment, the well established technique for strain measurements using electrical strain gauges can provide accurate estimations of the actual structural response. It is, however, not possible to mount gauges at all positions with critical details for large structures as bridges. The possibility of using a small scale monitoring system with few sensors has been investigated and a review of methods for predicting the response at unmeasured locations is presented in this report. A few selected methods, like multivariate regression and artificial neural networks (ANN), have been tested and evaluated on measured data from the Rautasjokk Bridge.

The use of an ANN for time history prediction is demonstrated and promising results are presented. However, the predictions are sensitive to the input data and questionable results were attained when the input deviated from the training set. For predictions based on stress range spectra, multivariate linear regression constitute a robust tool and provided a high accuracy for an example from the Rautasjokk Bridge.

This report also contains a presentation of the monitoring campaign of the Rautasjokk Bridge. The setup of the system and the management of data are described. The bridge is used for demonstrating the prediction methods and an advanced assessment approach based on linear elastic fracture mechanics. It enables a consideration of the measured response and a reliability based updating considering inspection results.

Sammanfattning

Med ett ökande antal broar som närmar sig sin förväntade livslängd, kommer krav på förbättrade metoder för tillståndsbedömning. Ekonomiska begränsningar och hållbarhetsskäl kommer att begränsa broförvaltares möjlighet att ersätta det stora antal broar som teoretiskt bedöms som osäkra. Fältmätningar erbjuder en möjlighet att bestämma den verkliga lasteffekten, och därmed bidra till en mer tillförlitlig tillståndsbedömning. Det medför att färre konservativa antaganden behöver göras vilket medför en högre noggrannhet i uppskattningen av den återstående livslängden.

För utmattningskontroll kan den väletablerade tekniken baserad på trådtöjningsgivare användas för att uppskatta den verkliga lasteffekten i en konstruktion. För stora konstruktioner som broar är det dock inte möjligt att montera givare på alla positioner med kritiska detaljer. Möjligheten att använda ett mätsystem med få givare har studerats och en granskning av metoder för uppskattning av lasteffekten i ej mätta positioner presenteras i denna rapport. Några få utvalda metoder, som t.ex. multivariat regressionsanalys och artificiella neurala nätverk (ANN), har testats och utvärderats för mätdata från järnvägsbron Rautasjökk Södra.

Skattning av tidshistorier med ANN demonstreras och lovande resultat redovisas. Skattningarna är dock känsliga för ingångsvärdena och tvivelaktiga resultat erhölls när ingångsvärdena avvek från urvalet för träning av nätverket. För skattningar baserade på spänningskollektiv utgör multivariat regressionsanalys ett tillförlitligt verktyg som visade hög noggrannhet för ett exempel från bron Rautasjökk Södra.

Denna rapport innehåller också en presentation av mätningarna på järnvägsbron Rautasjökk Södra. Mätsystemets uppbyggnad och genomförandet finns beskrivet. Bron används som fallstudie för demonstration av metoderna för uppskattning av lasteffekt och även för en avancerad metod för tillståndsbedömning baserad på linjärelastisk brottmekanik. Den senare möjliggör beaktande av uppmätt lasteffekt och en sannolikhetsbaserad uppdatering med avseende på resultat från inspektioner.

Preface

This report presents the work on fatigue deterioration performed within the project IP3-In2Track, financed by the Swedish Transport Administration (Trafikverket), with reference number TRV 2015/50535.

The research work has been performed by John Leander at the division of Structural Engineering and Bridges at KTH Royal Institute of Technology. The installation of the monitoring system on the Rautasjökk Bridge was performed by Mats Petersson and Erik Anderson from the MCE Lab at Luleå University of Technology (LTU).

Train configurations including axle loads and axle distances were provided by Dan Larsson at Damill AB from their measurements in Tornehamn, Björkliden.

The financial support provided by Trafikverket is gratefully acknowledged.

John Leander, July 3, 2018

Contents

Preface	v
Contents	vii
1 Introduction	1
1.1 Background	1
1.2 Aim and scope	6
1.3 Outline of report	6
2 Fatigue assessment	7
2.1 Variable amplitude loading	7
2.2 Linear damage accumulation	8
2.3 Linear elastic fracture mechanics (LEFM)	10
2.4 Summary	13
3 Methods for time history prediction	15
3.1 Theoretical influence lines	16
3.2 Kalman filtering	17
3.3 Artificial neural networks	18
3.4 Summary	20
4 Methods for spectrum prediction	23
4.1 Convergence rate	24
4.2 Multivariate linear regression	25
4.3 Neural network fitting	25
4.4 Summary	26
5 The Rautasjokk Bridge	27
5.1 Instrumentation	29
5.2 Monitoring program	29
5.3 Time history response	31
5.4 Stress range spectra	32
5.5 Fatigue assessment	37

5.6	Summary	40
6	Results of response predictions	41
6.1	Time history prediction	42
6.2	Stress range spectra predictions	43
6.3	Summary	44
7	Discussion and conclusions	47
7.1	Conclusions	47
7.2	Future research	48
	Bibliography	49
I	Instrumentation drawing	55

Chapter 1

Introduction

This report treats the assessment of steel bridges considering fatigue deterioration. It is aimed at the process of determining the remaining service life which is a delicate task where the uncertainties in resistance and load effect have to be considered. The governing regulations support a deterministic approach with characteristic values for the fatigue strength and conservative theoretical load models. This approach has shown to be adequate for design of new structures providing a sufficient safety against fatigue failure. For existing structures, however, the verification format can be too conservative showing insufficient resistance for apparently undamaged structures. This might lead to unnecessary interventions as repair or replacement. Another option is to engage more advanced theoretical methods to increase the accuracy of the service life prediction. This can include, e.g., in-service monitoring, advanced deterioration models, and probabilistic verification formats. This report is focused on the use of a small scale monitoring system with the purpose of decreasing the uncertainties in the estimated response.

1.1 Background

Figure 1.1 shows a photo of the Rautasjökk Bridge located along the iron ore railway line in Northern Sweden, between the city of Kiruna and the village Abisko. This bridge is a characteristic example of the main problem treated in this report. Theoretical assessments following the governing regulations have shown strong indications of an exhausted fatigue life (Häggström et al., 2016; Häggström, 2015). Decisive for the fatigue resistance are the welds to the top flange of the stringer beams where the lateral bracing is attached. An illustration of the connection is shown in Figure 1.2. No indication of damage has, however, been detected during inspections of this detail. When this happens, the bridge manager has to take a decision on how to secure the structural safety of the bridge. The initiation and propagation of a fatigue crack is a strongly nonlinear phenomenon and a small un-

detected crack can grow exponentially to a critical crack size. A cautious agent will engage practical interventions to improve the fatigue resistance or even to replace the bridge. But this will impose substantial costs, material consumption, and environmental impact. A theoretical upgrading using more advanced methods for assessment can be a more sustainable approach but it typically entails actions not supported by the governing regulations.



Figure 1.1: A photo of the Rautasjokk Bridge close to Kiruna in Sweden.

As an alternative approach to construction interventions to control or modify the risk for a structural failure, in-service monitoring is suggested in the standard ISO 13822 (ISO 13822, 2010). Practical aspects of performing monitoring are treated in, e.g., Kühn et al. (2008) and Sustainable Bridges (2007). How to implement measured response in a structural safety evaluation is, however, sparsely treated in guidelines and regulations. A rare exception is the Swedish regulation for assessment of existing structures (Trafikverket, 2017). It states that a stress range spectrum for fatigue assessment may be determined by in-situ measurements from one week of measurements or more.

In the research community, monitoring is often highlighted as a measure to increase the accuracy of service life predictions for bridges. A few selected examples are Connor and Fisher (2006), Zhou (2006), Liu et al. (2010), Leander et al. (2010), and Leander et al. (2015). All listed contributions treat fatigue assessment of steel bridges with a focus on the practical use of measured response. Despite several examples on how measurements can contribute with reduced uncertainties in the structural response, it is rarely requested as an intervention by structural owners.

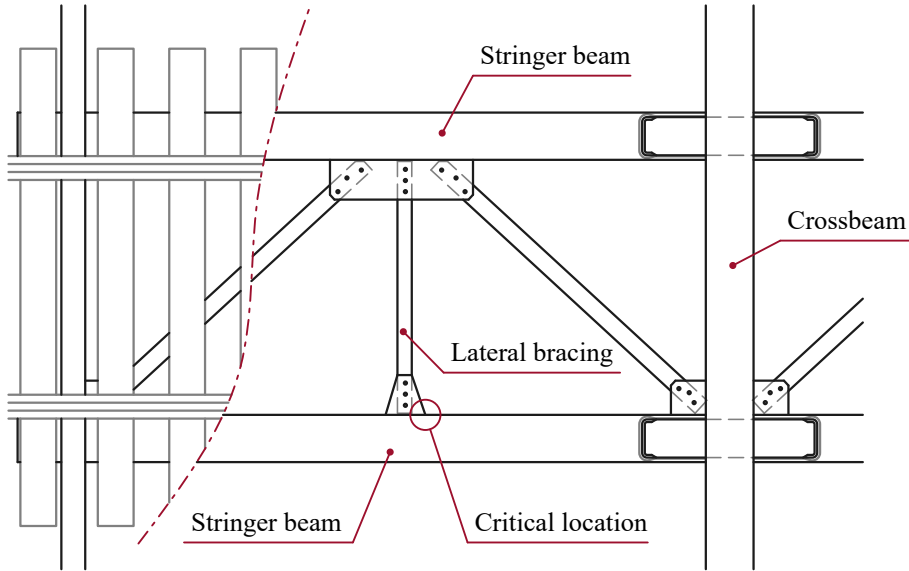


Figure 1.2: A sketch of the connection between the stringer beam and the lateral bracing.

This has initiated considerable research efforts on how to quantify the benefit of monitoring, e.g., the COST Action TU1402 *Quantifying the value of structural health monitoring*. One outcome of this action is the paper by Straub et al. (2017) exploring the concept of value of information (VoI) based on Bayesian decision theory. It enables an estimation of the benefit of a monitoring system before it is installed (Straub, 2014).

Even though the benefits of monitoring can be proven, practical obstacles remain before it can be established as a natural part of conventional assessments. The mounting of gauges, data acquisition, aggregation and interpretation are costly and require expert knowledge. For large monitoring campaigns, these parts will demand considerable management efforts, on top of the ordinary management of the bridge, causing a skepticism towards monitoring. Practitioners advocating monitoring, on the other hand, tend to highlight large monitoring campaigns with extensive numbers of sensors and large volumes of data collected. Some examples are the Tsing Ma Bridge and Stonecutters Bridge, both in Hong Kong, instrumented with hundreds of sensors (Wong, 2007).

In the current project, small scale monitoring systems have been the focus. The purpose was to investigate the utility of a small scale monitoring system for fatigue

assessment of steel bridges. Whether a few sensors at strategic positions can provide sufficient information to increase the accuracy in service life predictions at positions with no available measurements. This will require an approach with capacity to collect information from one location and make predictions at other locations. The general procedure is visualized in Figure 1.3. The objective is to determine the true response from the structure $y(t)$. However, only the response $x(t)$ and the load $F(t)$ can be measured. An estimate of $y(t)$, denominated by $\hat{y}(t)$, can be determined by some theoretical model and the measured information $x(t)$. This step is represented by the shaded box in Figure 1.3.

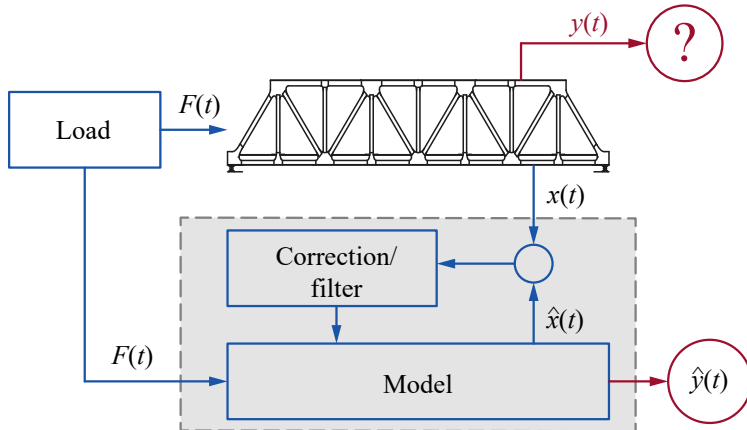


Figure 1.3: A conceptual scheme for predicting the unmeasured response $y(t)$.

In control theory, the shaded box in Figure 1.3 is typically called a *state observer* (Ogata, 2010) or a *state estimator*. It is a device or a computer program that observes measured output and estimates unmeasured state variables. The inputs to the observer are the control input $F(t)$ and the measured response $x(t)$, the former being the load in this case. The error between the measured response $x(t)$ and the estimated variable $\hat{x}(t)$ is used to continuously correct the model output and improve the performance of the observer. By compensating for the error between $x(t)$ and $\hat{x}(t)$, the accuracy of the estimation $\hat{y}(t)$ is expected to improve.

A Kalman filter (Kalman, 1960) is an example of a state observer. It has been used for estimation of the dynamic response for fatigue assessment by, e.g., Papadimitriou et al. (2011). They studied theoretical structural models subjected to unknown stochastic excitation. The fatigue assessment was performed based on the power spectral density (PSD) of the stress process.

Another example on the use of a Kalman filter is the investigation by Palanisamy

et al. (2015). A simply supported beam subjected to stochastic noise was studied numerically and experimentally. Measured accelerations, strains, and tilts were used to estimate the strain at unmeasured locations. A conclusion is that accelerations are unreliable for estimating quasi-static response due to low accuracy in low frequencies near 0 Hz. The use of strains generally produces higher noise levels in the prediction. A combination of input variables measuring different quantities gives more accurate estimations.

Maes et al. (2016) have evaluated three different techniques for estimating dynamic strain in an offshore monopile wind turbine. The purpose was to estimate strains at positions where direct measurements are impossible, by using a limited number of sensors. The measured response consisted of accelerations foremost, but a combination of measured accelerations and strains was also investigated. The three techniques were based on Kalman filtering, a joint input-state estimation algorithm, and a modal expansion algorithm. All three techniques rely upon modal decomposition with mode shapes and frequencies determined using a finite element model (FE model). Satisfactory results were reached for all technics and an interesting forecast is that accelerometers will replace and outperform regular strain sensors in a near future.

In the examples mentioned above (Papadimitriou et al., 2011; Palanisamy et al., 2015; Maes et al., 2016), the control input, $F(t)$ in Figure 1.3, was unknown and considered as stochastic white noise. For bridges, the control input is governed by a quasi-static load from traffic. If similar techniques for dynamic strain estimation as used in the examples above will work also for bridges remains to be investigated.

Iliopoulos et al. (2017) uses the term *virtual sensing* for the concept of estimating strains at unmeasured locations. A so-called multi-band modal decomposition and expansion technique was used in a study of an offshore monopile wind turbine, the same structure as treated by Maes et al. (2016). The multi-band approach was adopted to capture the quasi-static response in the frequency range from 0 to 0.2 Hz (Iliopoulos et al., 2017). A FE model was used to determine the dynamic mode shapes and a static mode for the very low-frequent strain contributions. Measured strains and accelerations were then used together with the theoretical modes to predict the response at unmeasured locations.

The term virtual monitoring has been used by Hajializadeh et al. (2017) for response estimation using monitoring in combination with an updated finite element model. The measured response was used for both bridge weigh-in-motion (B-WIM) and for updating of the model. The actual traffic load and the model was then used for predicting the response at unmeasured locations. The concept builds upon a short term monitoring campaign to determine the conditions for the assessment. Unlike the use of a *state observer*, the estimation is then performed using the updated FE model only.

Model updating is a research area of itself contiguous to the issue of response estimation. It is, however, not treated in this report. This project has been aimed at the use of monitoring as the main source for response estimation. Nevertheless, for the interested reader, a recent contribution related to fatigue assessment has been presented by Pai et al. (2018) looking at different methods for data interpretation and model updating.

1.2 Aim and scope

The aim of the research project was to facilitate the use of monitoring for fatigue assessment of existing steel bridges. The use of monitoring is expected to increase the accuracy of service life predictions leading to a postponement of interventions as repair and replacement.

The objectives with the project were:

- A survey of methods for response prediction at unmeasured locations.
- Initiation of a long term monitoring campaign for the Rautasjokk Bridge using a small scale monitoring system.
- A superficial fatigue assessment of the Rautasjokk Bridge based on measured and predicted response.

This investigation was limited to stress prediction in steel bridges or similar structures, where the quasi-static response caused by heavy loading is dominating. A linear elastic structural behaviour was assumed, and assessment considering high cycle fatigue.

1.3 Outline of report

Chapter 2 contains a brief review of methods for fatigue assessment of existing steel bridges. It is focused on the implementation of measured response. Measured time histories and relations between measured response at different locations in the time domain are treated in Chapter 3. The derivation of stress range spectra and questions related to the stability and relations between different gauge locations are treated in Chapter 4. The case study, the Rautasjokk Bridge, is presented in Chapter 5. It contains also a description of the monitoring campaign and the interpretation of the data. Some of the prediction methods treated in Chapters 3 and 4 have been applied to the measured data from case study and the result is presented in Chapter 6. The report is ended with a discussion and conclusions in Chapter 7.

Chapter 2

Fatigue assessment

For existing bridges, the main purpose of a fatigue assessment is to determine the residual service life. For how many more years a bridge can sustain the structural safety at an acceptable level. In this chapter, some of the most established methods for fatigue assessment are briefly described, with focus on how to incorporate measured response. A more thorough review of assessment methods can be found in, e.g., the publication by Kühn et al. (2008). The fundamentals in fatigue of materials can be found in textbooks by, e.g., Maddox (1991), Suresh (1998), and Stephens et al. (2001).

2.1 Variable amplitude loading

Passing vehicles on bridges inevitably cause variable amplitude stresses and typically a large number of cycles. Large variations in vehicle types render a broad distribution of stress ranges while a homogenous traffic gives a narrow distribution. In the case of measurements, the distribution can be determined using a cycle counting technique as, e.g., the rainflow counting method (Amzallag et al., 1994). Figure 2.1 shows examples of stress range spectra from the Old Lidingö Bridge and the Söderström Bridge, both located in Stockholm, Sweden. The former bridge carries the traffic on the Lidingöbanan consisting of a specific type of tram vehicle. The latter is loaded by a mixture of trains travelling on the main railway line going south from Stockholm Central Station.

Figure 2.1(a) shows that even for a traffic situation with only one type of vehicle, the stress range distribution has a significant dispersion. This is caused by differences in axle loads due to the number of passengers and the interaction with low amplitude loads as wind and vehicles on the adjacent cycle path.

The variable amplitude loading is often considered in conventional assessments

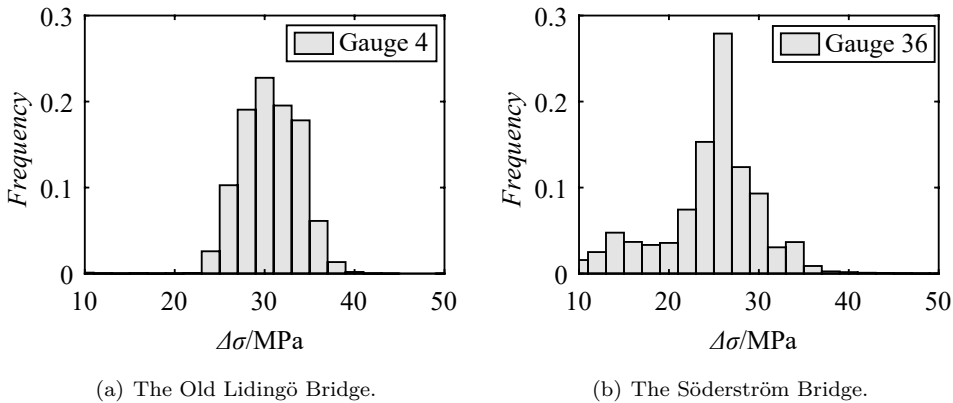


Figure 2.1: Stress range spectra based on strain measurements on stringer beams.

by the use of an equivalent stress range. The Eurocode EN 1993-2 (CEN, 2009) suggests a damage equivalent stress range $\Delta\sigma_{E2}$ related to a fixed number of 2 million cycles. In research literature, an equivalent stress range is often used defined as (Schilling and Klippstein, 1977)

$$\Delta\sigma_e = \left(\sum_i f_i \Delta\sigma_i^m \right)^{1/m} \quad (2.1)$$

where f_i is the normalised number of cycles in stress range $\Delta\sigma_i$, and m is the slope of the considered S - N curve. It builds on the Palmgren-Miner rule for linear damage accumulation (Palmgren, 1924; Miner, 1945). The equivalent stress range is readily calculated when the S - N curve has a single slope. However, if a bilinear curve is used as suggested in EN 1993-1-9 (CEN, 2006) and a fatigue limit is considered, the benefit of using an equivalent stress range is lost. It is then preferable to include the complete stress range spectrum in the verification format as described in the following sections.

2.2 Linear damage accumulation

The verification format in the governing regulations for fatigue assessment of bridges is based on the Palmgren-Miner rule for linear damage accumulation. It has been the prevailing format since the 1970ies in most regulations (Jarfall, 1974; Dexter et al., 2004).

Deterministic verification

The conventional verification is defined as (CEN, 2009)

$$\gamma_{Ff} \Delta\sigma_{E2} \leq \frac{\Delta\sigma_C}{\gamma_{Mf}} \quad (2.2)$$

where γ_{Ff} and γ_{Mf} are partial safety factors; $\Delta\sigma_{E2}$ is the damage equivalent stress range representing the load effect; and $\Delta\sigma_C$ is the fatigue strength at 2 million cycles. This condition determines if the fatigue resistance is sufficient in comparison to $\Delta\sigma_{E2}$ calculated for a specified conservative load model.

If the verification according to (2.2) indicates an insufficient resistance, or if the model for determining $\Delta\sigma_{E2}$ is judged inappropriate, EN1993-1-9 (CEN, 2006) supports the use of the Palmgren-Miner rule. The condition for the verification is defined as

$$D_{Ed} = \sum_{i=1}^N \frac{n_i}{N_{Rd,i}} \leq 1 \quad (2.3)$$

where n_i is the number of cycles in stress range $\Delta\sigma_i$ and $N_{Rd,i}$ is the fatigue endurance for the same stress range. The summation should be performed for all stress ranges $i = 1, \dots, N$. For a linear $S-N$ curve, the fatigue endurance can be calculated as

$$N_{Rd} = 2 \times 10^6 \left(\frac{\Delta\sigma_C}{\gamma_{Ff}\gamma_{Mf}\Delta\sigma} \right)^m \quad (2.4)$$

The linear relation can be readily extended to a bilinear formulation as described in EN 1993-1-9.

In a design situation, the details of the future traffic conditions are unknown which makes the format described by (2.2) practical. For assessment of existing bridges, this format is often too conservative making it difficult to prove a sufficient resistance. Furthermore, it doesn't provide any quantitative measure of the remaining service life. With damage accumulation using (2.3), the actual traffic history can be taken into consideration. It also provides a relation between the damage and the number of accumulated cycles, which in turn is associated to the service life.

From measurements of strain using, e.g., uniaxial electrical strain gauges, the stress history can be calculated by Hooke's law, which in turn can be analysed with a cycle counting method. This will give a stress range spectrum describing the number of cycles in each stress range as shown in Figure 2.1. This result can then be included directly in the verification format (2.3).

Probabilistic verification

The verification formats represented by (2.2) and (2.3) are based on safety factors and conservative assumptions for the load and resistance. A more profound

evaluation of the structural safety can be achieved by using a probabilistic format allowing an explicit consideration of the uncertainties. Probabilistic methods for assessment are typically endorsed by the governing regulations, see e.g. 3.5(5) i EN 1990 (CEN, 2010). However, none or very limited instructions on how to proceed in practice are provided. The Joint Committee of Structural Safety (JCSS) has tried to overcome this deficiency by developing a Probabilistic Model Code (JCSS, 2011). It describes superficially how to perform a probabilistic fatigue assessment.

For linear damage accumulation, it is convenient to formulate a limit state equation based on accumulated damage as

$$g(\mathbf{x}) = \delta - \sum_{i=1}^N \frac{n_i}{N_{R,i}(\mathbf{x})} \quad (2.5)$$

in which δ is a stochastic variable representing the resistance measured in damage and \mathbf{x} is a vector containing the other basic variables. The fatigue endurance $N_{R,i}(\mathbf{x})$ can be expressed as

$$N_R(\mathbf{x}) = K (C_S \Delta \sigma)^{-m} \quad (2.6)$$

where K and m describe the intercept and the slope of the S - N curve, respectively, and C_S is a model uncertainty factor related to the stress. Guidance on how to assign statistical properties to the variables can be found in JCSS (2011).

A state of failure is defined as $g(\mathbf{x}) \leq 0$ and the probability of failure as

$$P_f = P [g(\mathbf{x}) \leq 0] \quad (2.7)$$

The probability of failure is associated to the reliability index β as $P_f = \Phi(-\beta)$, where $\Phi(\cdot)$ is the standard normal distribution. The probability of failure or the associated reliability index can be estimated using conventional methods for reliability analysis like, e.g., the first order reliability method (FORM), the second order reliability method (SORM), Monte Carlo simulation, or by some more refined simulation technique.

The level of safety is assessed against an acceptable probability of failure. For fatigue of existing structures, a target value of 10^{-3} is suggested in the standard ISO 13822 for not inspectable details. In combination with inspections a value of 10^{-2} is suggested. Expressed in reliability index the associated values are $\beta = 3.1$ and $\beta = 2.3$, respectively. These values are stated for a reference period equal to the intended remaining service life.

2.3 Linear elastic fracture mechanics (LEFM)

The initiation and propagation of a fatigue crack is a pronounced nonlinear phenomenon as shown schematically in Figure 2.2. By linear damage accumulation,

the degree of damage can be simplistically estimated but it does not reflect the true damage progress. A more realistic description can be reached by using linear elastic fracture mechanics (LEFM). It provides a mathematical model to relate the crack size to the number of cycles.

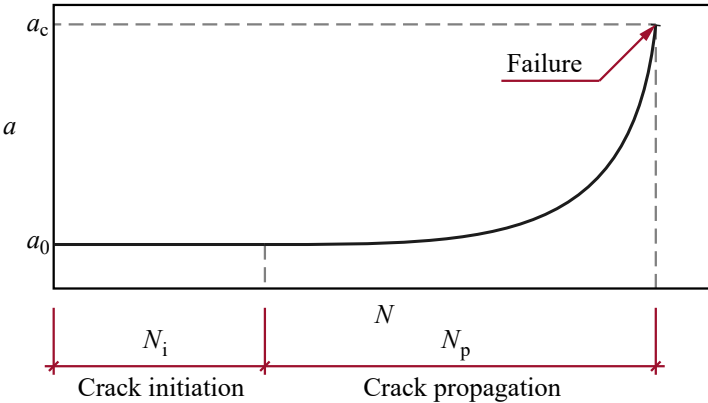


Figure 2.2: The schematic relation between the crack size a and the total fatigue life $N_c = N_i + N_p$.

LEFM is sorted as a damage tolerant method which is not supported for assessment of steel bridges in the governing regulations. However, detailed guidance can be found in the British Standard BS 7910 (BSI, 2013).

The crack driving force is the stress intensity range which can be formulated as

$$\Delta K(a) = \Delta\sigma\sqrt{\pi a} Y(a) M_k(a) \quad (2.8)$$

where a is the crack depth, $\Delta\sigma$ is the stress range, $Y(a)$ is a geometry correction factor representing the base component, and $M_k(a)$ is a stress magnification factor considering the influence of possible on-welded attachments (Hobbacher, 1992). The number of cycles to failure N_c (\mathbf{x}) is calculated by integrating a crack growth rate as

$$N_c = \int_{a_0}^{a_c} \left(\frac{da}{dN} \right)^{-1} da \quad (2.9)$$

where a_0 and a_c are the initial crack depth and the critical crack depth representing the final failure of the component, respectively. The crack growth rate is typically described by the well-known Paris law (Paris et al., 1961)

$$\frac{da}{dN} = A (\Delta K)^m \quad (2.10)$$

where A and m are constants dependent on the material and loading conditions.

Deterministic verification

An assessment based on LEFM requires more variables than the method based on linear damage accumulation. Since no support is available in the regulations for bridges, it can be troublesome to find appropriate characteristic values. For the material parameters A and m in the crack growth rate, conservative values are suggested in BS 7910. An initial crack depth of $a_0 = 0.1$ mm, and for semi-elliptic surface cracks, an aspect ratio of $a/c = 0.1$, are suggested by Hobbacher (2016). To comply with the general safety format in the Eurocode, the stress range $\Delta\sigma$ in (2.8) should be multiplied with the partial safety factors γ_{Ff} and γ_{Mf} .

For variable amplitude loading, the integration in (2.9) needs to be performed incrementally for the different stress ranges. The order of the stress ranges can have a noticeable influence on the resulting total fatigue life. It has, however, been shown by Leander and Al-Emrani (2016) that for an ordinary mixture of vehicles, the loading can be considered as an ergodic process and an expected crack growth rate can be used defined as

$$E \left[\frac{da}{dN} \right] = A E [\Delta\sigma^m] (\gamma_{Ff} \gamma_{Mf} \sqrt{\pi a} Y(a) M_k(a))^m \quad (2.11)$$

where $E[\cdot]$ denotes the expected value. This allows a reduction of the stress range spectrum to an expected value $E[\Delta\sigma^m]$ in the calculation of the crack growth rate, which in turn greatly simplifies the integration in (2.9).

Probabilistic verification

A limit state equation based on LEFM can be expressed based on the number of cycles as

$$g(\mathbf{x}) = N_c(\mathbf{x}) - N \quad (2.12)$$

where $N_c(\mathbf{x})$ is the number of cycles to failure related to the crack growth rate as defined by (2.9) and N is the total number of cycles at the studied point in time. The vector \mathbf{x} contains the variables of the deterioration model. The probability of failure is defined by (2.7).

The expected crack growth rate can be estimated as suggested by JCSS (2011)

$$E \left[\frac{da}{dN} \right] = A E [\Delta\sigma^m] (C_S C_{SIF} \sqrt{\pi a} Y(a) M_k(a))^m \quad (2.13)$$

where C_S and C_{SIF} are model uncertainties for the nominal stress and the stress intensity factor, respectively.

Reliability updating

An assessment based on probabilistic fracture mechanics enables an updating of the probability of failure considering results from inspections. A detection event

can be expressed as

$$H_D(\mathbf{x}) = a(\mathbf{x}, N_i) - a_d \quad (2.14)$$

where $a(\mathbf{x}, N_i)$ is the estimated crack size at cycle N_i considering the stochastic variables in \mathbf{x} . A lower limit of detectability denoted a_d should be considered as a stochastic variable and is typically described by a probability of detection (PoD) curve. An event $H_D(\mathbf{x}) \leq 0$ indicates that no crack is detected which is the preferable outcome of an inspection. The estimated probability of failure can then be updated considering the detection event as

$$P_f^U = P[g(\mathbf{x}) \leq 0 | H_D(\mathbf{x}) \leq 0] = \frac{P[g(\mathbf{x}) \leq 0 \cap H_D(\mathbf{x}) \leq 0]}{P[H_D(\mathbf{x}) \leq 0]} \quad (2.15)$$

A more elaborate description of the procedure can be found in, e.g., the textbook by Madsen et al. (2006) and in the paper by Leander et al. (2018).

A challenge is to assign a realistic PoD curve for the the inspection method and the prevailing conditions at site. Established curves for inspection of bridges do not exist but recommendations for offshore structures are given by DNV GL (2015). A general distribution function for PoD curves is suggested as

$$P(x) = 1 - \frac{1}{1 + \left(\frac{x}{X_0}\right)^b} \quad (2.16)$$

where x is the visible crack length for visual inspections and the crack depth a for other methods. The variables X_0 and b depends on the inspection method and the conditions during the inspection.

2.4 Summary

A verification format based on linear damage accumulation is straight forward to use and is supported by the governing regulations, specifying a safety format based on partial safety factors. Measured response can be considered using a cycle counting method like rainflow analysis and the well-known Palmgren-Miner rule.

For a more profound assessment of the remaining service life, probabilistic LEFM is suggested. It enables an assessment of the probability of failure and allows a reliability updating considering results from inspection. By connecting the theoretical assessment to practical in-situ inspections, a significant increase in the accuracy of the assessment can be expected. And if no crack is detected – an increase in service life.

Chapter 3

Methods for time history prediction

Two examples of measured time responses for a train passing the Rautasjokk Bridge are shown in Figure 3.1. One line shows the result for a gauge at a stringer beam and the other for a gauge at one of the first diagonals of the main truss. Firstly, the figure shows that the response is strongly dependent on the location of the gauge. This is related to the influence length of the studied position in the structure. Secondly, the response is dominated by the static weight of the vehicle. Dynamic oscillations are detectable as a noise around the quasi-static response. It should be noted that the response has been filtered with a low pass cut-off set to 10 Hz.

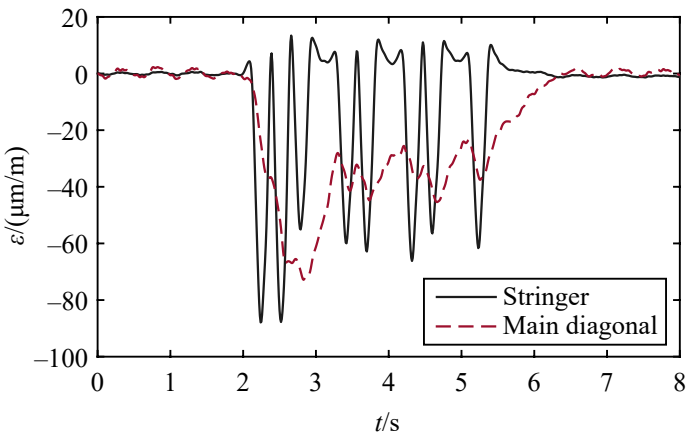


Figure 3.1: Measured strains for a passage of an Intercity train on the Rautasjokk Bridge.

The dominance of the quasi-static response indicated in Figure 3.1 motivated the choice to neglect the influence of dynamics in the theoretical parts of this chapter. It should, however, be noted that even a small dynamic amplification can have a significant influence on the fatigue life due to the exponential relation to the stress range. See Chapter 2. The obvious approach to eliminate the uncertainty related to the influence of dynamics is to do measurements. Time histories from measurements will be treated superficially in the current chapter but more extensively in relation to the study of the Rautasjökk Bridge in Chapter 5.

3.1 Theoretical influence lines

An influence line represents the response at a specific location to the passage of a moving load. Figure 3.2 shows the influence lines for an idealized continuous beam in eight spans. It can be viewed as a simplified model of a stringer beam.

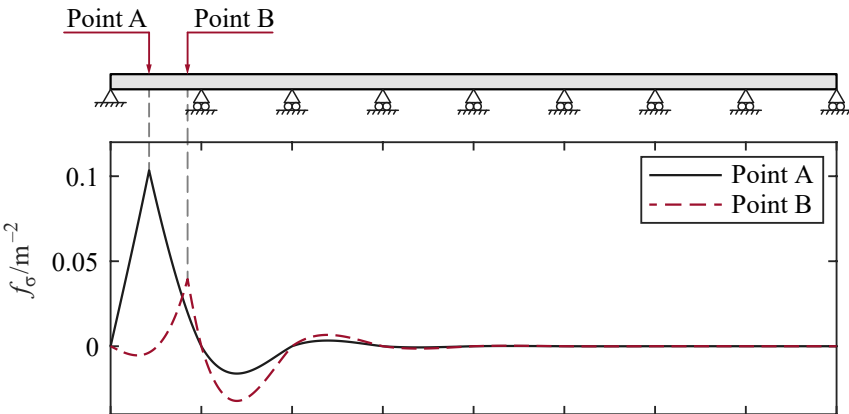


Figure 3.2: Influence lines for the stress at two positions along a continuous beam in eight spans.

If the influence line at a specific point can be determined with high accuracy, the true response caused by the passage of a vehicle can be determined based on the axle positions d_i and the weights F_i for the axles $i = 1, \dots, N_a$ as

$$\sigma(x_1) = \sum_{i=1}^{N_a} f_\sigma(x_1 - d_i) F_i \quad (3.1)$$

where $f_\sigma(\cdot)$ is the function for the influence line, x_1 is the position on the bridge for the first axle of the vehicle, and d_i is the distance from the first axle to axle i of the vehicle. The response $\sigma(x)$ can be readily recalculated to a time history $\sigma(t)$ by scaling the x-axis with the speed of the vehicle.

Figure 3.3 shows the estimated time history using the idealized influence line for Point A in Figure 3.2 and the vehicle properties for the same passage as shown in Figure 3.1. There is an overall agreement between the time histories in the figure. The most pronounced difference is the peak values caused by each axle in the theoretical model, which are not appearing in the measured response. An evaluation of the equivalent stress range according to (2.1) gave $\Delta\sigma_e = 15.5 \text{ MPa}$ and $\widehat{\Delta\sigma}_e = 16.2 \text{ MPa}$ for the measured and estimated stresses shown in Figure 3.3, respectively.

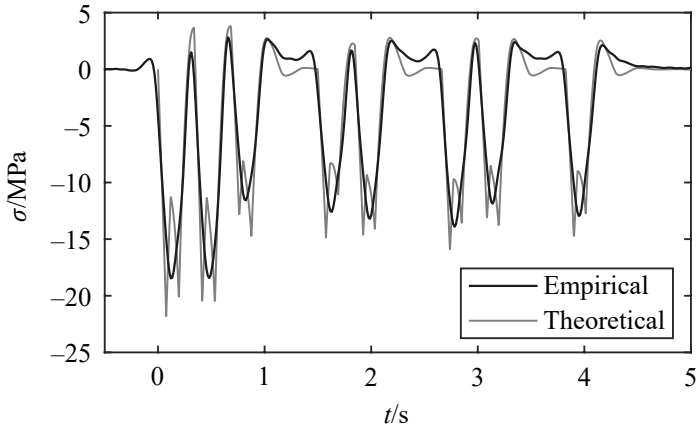


Figure 3.3: Measured and estimated response of a train passage for Point A in Figure 3.2.

The overall acceptable agreement between the measured and the estimated stresses shown in Figure 3.3 cannot be expected in general. The actual statical system of the stringers is close to the idealized model in Figure 3.2 but, the behaviour of other structural members may be far more difficult to predict. With access to measurements, a theoretical model can be updated to increase the accuracy. However, the true response at unmeasured locations will still be afflicted with uncertainties.

3.2 Kalman filtering

Kalman filtering has been used by, e.g., Maes et al. (2016) for fatigue life prediction of an offshore steel structure. The response at the mud-line below the sea level, where it is difficult to mount sensors, was predicted using measured response above the sea level. Their approach was based on a modal decomposition together with Kalman filtering to estimate the dynamic strains.

A Kalman filter can be used as a tool for estimating the state of a linear dynamic

system subjected to a stochastic excitation, using measurements to increase the accuracy of the estimation (Grewal and Andrews, 2015). The shaded box in Figure 1.3 visualizes the concept of a Kalman filter. The accuracy of the prediction of $y(t)$ using a theoretical model can be corrected (filtered) based on the difference between the measured and predicted response $x(t)$. The prediction at time t_k for a discrete-time model can be formulated mathematically as

$$\hat{y}_{k(+)} = \hat{y}_{k(-)} + \bar{K}_k (x_k - H_k \hat{y}_{k(-)}) \quad (3.2)$$

where $\hat{y}_{k(-)}$ represents the a priori value of the the estimation (before the information in the measurements is used), $\hat{y}_{k(+)}$ is the a posteriori value, \bar{K}_k is the so-called Kalman gain, x_k is the measured response at time t_k , and H_k is a measurement sensitivity matrix which relates the measured response x_k to the sought response y_k . A rigorous derivation of the mathematics behind Kalman filtering can be found in, e.g., the textbook by Grewal and Andrews (2015).

A limitation of the original Kalman filter is the fundamental assumption of a linear relation between y and x . This is fulfilled in a dynamic analysis by using modal superpositioning as, e.g., by Maes et al. (2016). However, when a quasi-static behaviour is governing and the relation between different points is nonlinear, the fundamental condition of the method is not fulfilled. Extended versions of the Kalman filter approach has been developed for nonlinear systems, see e.g. Chatzi and Smyth (2015), but this is beyond the scope of the current study.

3.3 Artificial neural networks

An artificial neural network (ANN) allows a modelling of both linear an nonlinear systems. It can be used as a data-driven non-parametric model which do not require restrictive assumptions on the underlying process from which the data is collected (Zhang, 2012). Figure 3.4 shows a typical feedforward neural network for time series prediction modified after Zhang (2012). While the typical application concerns forecasts of the input variable ($\hat{x}(t+1)$), the application herein concerns the prediction of an unmeasured response ($y(t)$).

The ANN in Figure 3.4 is called a multilayered feedforward network (Haykin, 2009) consisting of one input layer, one or several hidden layers and one output layer. For time series prediction the neurons in the input layer are fed with past and sometimes future observations from the measured data. The neurons in the hidden layers process the information from the input layer and delivers a prediction to the output layer.

Before the network can be used for prediction it has to be trained (learned). To establish the connection between the unmeasured and measured response, a supervised learning procedure is needed. This can be based either on short term

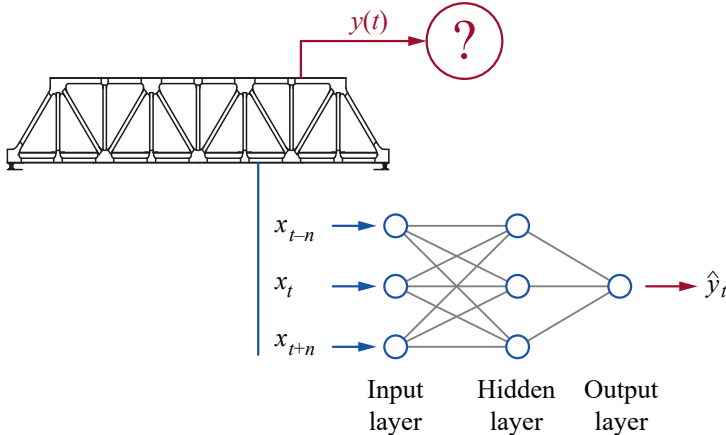


Figure 3.4: A multilayered feedforward artificial neural network for response prediction.

measurements on several positions, or by using a theoretical model reflecting the relation between the positions. More information about training (learning) can be found in, e.g., the publications by Haykin (2009), Zhang (2012), and Hagan et al. (2014).

Besides the training of the network, Zhang (2012) highlights the importance of the network design. The number of layers, the number of neurons in each layer, and the connections between the neurons may have a significant influence on the prediction accuracy. The number of neurons in the input layer is mentioned as one of the most important choices. This comprises the number of past and future observations and the time step between them. Using a machine learning method as ANN is often described as a black box approach, however, a successful result typically requires a careful consideration of the data characteristics and the design of the network.

To demonstrate the use of a ANN, the relation between the points A and B in Figure 3.2 has been studied. A time delay neural network was designed using the Neural Network Toolbox in Matlab. The number of input neurons was set to 41 representing the number of observations $x_{t-20}, x_{t-19}, \dots, x_{t+20}$, one hidden layer of size 10 was considered, and one output neuron representing y_t was assigned. The network was trained using Levenberg-Marquardt backpropagation (Hagan and Menhaj, 1994) for one single passage of a short Intercity train with 16 axles. The time history for the training set is shown in Figure 3.5 with the response at points A and B as $x(t)$ and $y(t)$, respectively.

The trained network was used for predicting the response at point B of another

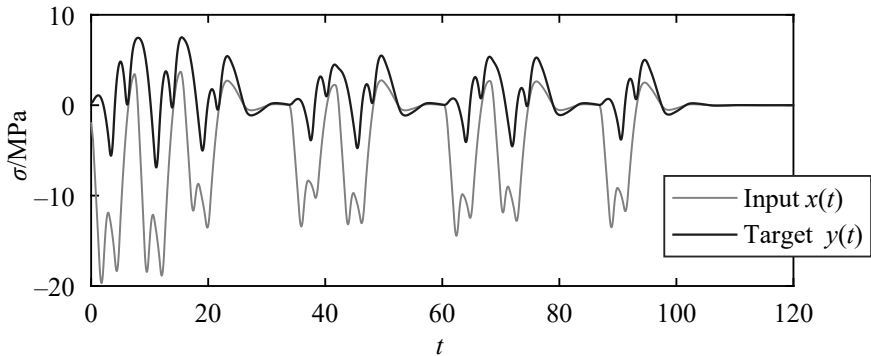


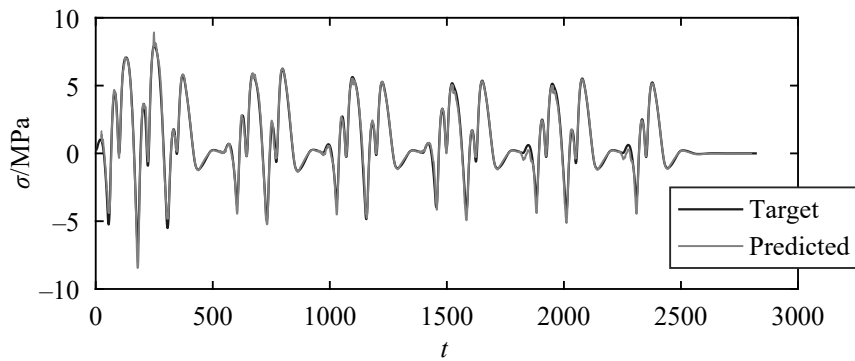
Figure 3.5: Calculated time histories for the passage of an Intercity train with 16 axles used for training of a ANN.

train passage using the input from point A only. The result is shown in Figure 3.6 together with the analytically calculated target response. A relatively good agreement was achieved for the train passage in Figure 3.6(a). The configuration of this train was similar to the train passage used for training. For another type of train, as shown in Figure 3.6(b), the predicted response differs significantly. This highlights the need to include several train passages of different types in the training phase to reach a more versatile network. It should also be noted that both the training and the verification was performed using the theoretical influence lines from Figure 3.2. In practice, the idea is to use a theoretical model for training but measured response for prediction.

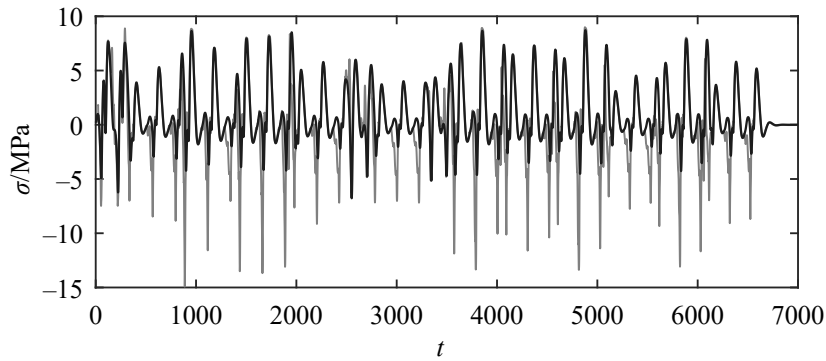
3.4 Summary

For fatigue assessment the time history response is required for derivation of the stress range spectrum. The conventional approach is to use a theoretical model and a simplified load to derive conservative estimations. This is exemplified in Section 3.1 by the use of influence lines from a simplified theoretical model. With a more complex and detailed model, the response at any position of a bridge can be estimated.

If the accuracy of the theoretical estimation is questioned, in-service measurements are recommended. For practical reasons it is not possible to mount sensors at all critical locations. For this reason, Kalman filtering and machine learning have been reviewed as tools to predict the response at unmeasured locations. While the applicability of Kalman filtering is limited due to the assumption of a linear system, machine learning based on artificial neural networks appears promising.



(a) The passage of a train with 24 axles.



(b) The passage of a train with 74 axles.

Figure 3.6: Predicted response using the trained network.

Chapter 4

Methods for spectrum prediction

A cycle counting procedure of a time history produces an aggregated response in the form of a stress range spectrum. A time history recorded by dense sampling will be reduced to a vector containing the number of cycles in each stress range. This reduction of data is beneficial considering data transfer by wireless communication and storage. It also motivates a study on how the response at unmeasured locations can be predicted through relations between stress range spectra, as an alternative to time histories as in Chapter 3. The transformation of the stress range spectrum from point y to point x can be expressed as a matrix operation

$$\mathbf{s}_y = \mathbf{T} \mathbf{s}_x \quad (4.1)$$

where \mathbf{s} is a row vector of the number of stress ranges and \mathbf{T} is a transformation matrix.

In the master thesis by Lundman and Parnéus (2018), a deterministic approach to establish the transformation matrix was developed. It is based on a finite element model of the bridge and stepwise evaluations of individual stress ranges. The approach was evaluated on spectra from the measurements on the Rautasjokk Bridge. A verification against the measurements showed a deviation in fatigue damage around 20 % for gauge locations at members with similar behaviour. For gauges mounted on members with large differences in behaviour, e.g., a stringer beam and the main truss, the deviation became inadmissible. A challenge for members with long influence lines is that each vehicle/train causes one or a few stress ranges that can vary significantly in amplitude. In the case of fatigue assessment, even a few but large stress range amplitudes may greatly influence the fatigue life. This is related to the convergence of stress range spectra treated in Section 4.1.

The deterministic approach developed by Lundman and Parnéus (2018) resulted in a sparse transformation matrix neglecting the correlation between different stress

range levels. To explore the influence of correlations two statistical methods have been reviewed in this chapter. Firstly, a methods based on conventional multivariate regression analysis is treated in Section 4.2. Secondly, a method based on machine learning for model fitting is treated in Section 4.3.

4.1 Convergence rate

Members with a short influence length will be subjected to many load repetitions caused typically by every axle or bogie of the vehicles. Hence, for a collection of vehicle passages, the member will rather quickly have sensed a large population of axle loads and reached a close to static stress range spectrum. In contrast, looking at a member with a long influence line, one stress range will depend on the weight of several axle loads and perhaps the whole vehicle. This means that the stress range spectra inevitable will converge at a slower rate and also suffer from a larger scatter. This relation have been detected in results from practical measurements in the paper by Leander and Karoumi (2012).

The equivalent stress range as defined by (2.1) can be used to study the progress of the convergence. As a tentative example, samples from a stress range distribution following a uniformly distribution between 10 MPa and 60 MPa have been generated. For member A, one train passage is assumed to render 10 cycles, while for member B, only one cycle is assumed. This gave the progress of the equivalent stresses as shown in Figure 4.1 calculated with the slope variable assigned to $m = 3$. It is apparent in the figure that the equivalent stress range for member B need more passages before a converged level is reached. The same tendency can be expected for the accumulated damage.

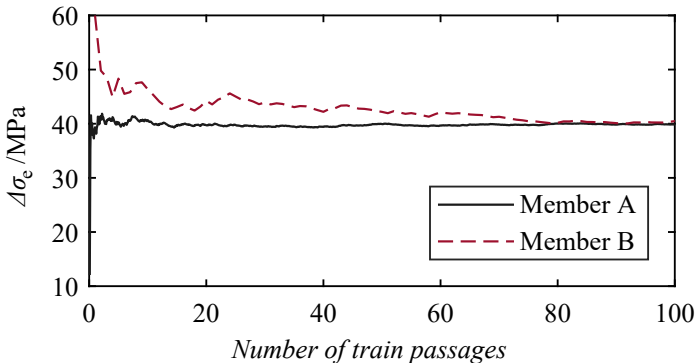


Figure 4.1: An example on the progress of the equivalent stress range $\Delta\sigma_e$.

4.2 Multivariate linear regression

In multiple regression, one response variable y is predicted based on multiple predictor variables \mathbf{x} . In *multivariate* regression, the response is also composed by multiple variables. The regression model can be expressed mathematically as (Olive, 2017)

$$\mathbf{y}_i = \mathbf{B} \mathbf{x}_i + \boldsymbol{\epsilon}_i \quad (4.2)$$

for $i = 1, \dots, n$ observations (cases) with y_1, \dots, y_m response variables, x_1, \dots, x_p predictor variables, and the error $\boldsymbol{\epsilon}$. When \mathbf{x}_i and \mathbf{y}_i represent different stress range spectra, the length of the vectors are typically the same. In matrix form, the model can be written as

$$\mathbf{Y} = \mathbf{B} \mathbf{X} + \mathbf{E} \quad (4.3)$$

The regression involves estimating the coefficient matrix \mathbf{B} , which is an estimation of the transformation matrix \mathbf{T} in (4.1). Methods for fitting the multivariate model are described, e.g., in the textbook by Olive (2017). It can be performed in practice by the function `mvregress` in Matlab.

The prediction of a stress range spectrum at an unmeasured location can be divided into two phases;

1. The coefficient matrix \mathbf{B} is determined by fitting the model to the response spectrum \mathbf{Y} and the predictor spectrum \mathbf{X} determined from, e.g., a theoretical model;
2. The coefficient matrix is used for predicting a new spectrum $\hat{\mathbf{s}}_y$ from a measured response \mathbf{s}_x .

The approach is demonstrated in Section 6.2.

4.3 Neural network fitting

As in Section 3.3 a method based on an ANN has been evaluated but this time, to find a transformation model to predict a stress range spectrum at an unmeasured location. The phases for prediction follows the same procedure as for the regression analysis outlined in Section 4.2 with the difference that the determination of the coefficient matrix is replaced by the training of a neural network.

The ANN will in this case be trained with $i = 1, \dots, n$ stress range spectra from a theoretical model where i counts individual train passages or time units like days. A network for this purpose can be designed using the `fitnet` function in the Neural Network Toolbox in Matlab.

The approach is demonstrated in Section 6.2.

4.4 Summary

By cycle counting, a dense stress history can be reduced to a stress range spectrum which usually is far less in storage size. This can be utilized in, e.g., wireless communication to reduce the amount of data being transmitted. The number of cycles in each stress range reflected by the spectrum is the response required for fatigue assessments. Predictions of the response at unmeasured locations through the stress range spectra can thereby be an expedient alternative to predictions through time histories.

A spectrum is composed of a discrete distribution of cycles. This entail a need for multidimensional approaches for connecting one spectrum to another. For this purpose the use of multivariate linear regression and artificial neural networks are suggested.

Chapter 5

The Rautasjokk Bridge

The Rautasjokk Bridge is located on the railway line between the city of Kiruna and the village Riksgränsen, see Figure 5.1. It has the identification number 3500-2118-1(1) in the Swedish bridge and tunnel management system BaTMan (Trafikverket, 2004). Its original abutments were built 1902 and the present superstructure 1962. A photo of the bridge is shown in Figure 1.1.



Figure 5.1: A map of northern Sweden and the iron ore line between Boden and Riksgränsen.

The load carrying structure consists of two simply supported parallel steel trusses

with a span length of 33 meters. The single track is carried by stringer beams, which in turn spans between crossbeams. A sketch of the structure is shown in Figure 5.2.

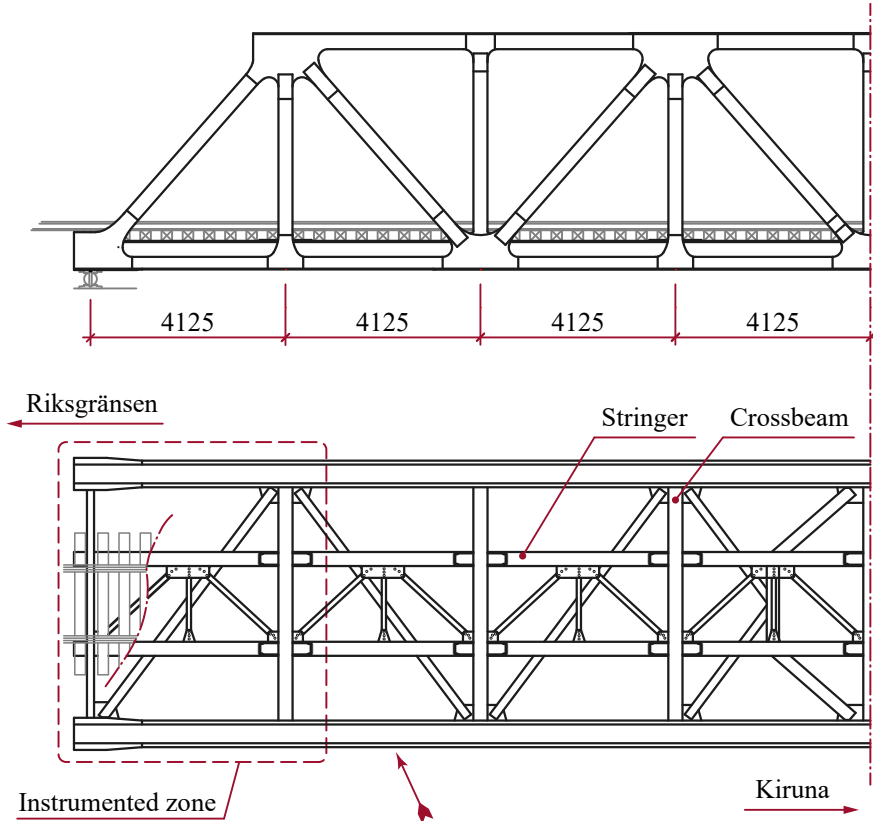


Figure 5.2: A sketch of the load carrying structure for the Rautasjokk Bridge.

Assessments of the bridge have indicated that the fatigue life is exhausted. The critical details are according to Häggström (2015), the connections of the lateral bracing to the stringer beams, the rolled section of the crossbeams, and the riveted connection of the stringer beams to the crossbeams. The first detail is the most critical, however, no cracks have been found during inspections. In the ultimate limit state, the bridge has sufficient resistance for axle loads up to 34 tons.

The discouraging results of the conventional assessments have led to more detailed assessments using in-service measurements and a verifications based on structural hot spot stress (Häggström et al., 2016). Even so, the results still indicate an exhausted fatigue life.

The Rautasjokk Bridge was selected as a case study for the current project because it is representative for many other similar railway bridges in Sweden and internationally. It is also considered as a fatigue critical bridge due to the results of the previous assessments and because of the high load levels from the iron ore trains. The railway line between Boden and Riksgränsen is the only line in Sweden allowing axle loads of 30 tons.

5.1 Instrumentation

In October 2017, the bridge was instrumented with six uniaxial strain gauges and two accelerometers. Only the results from the strain gauges will be treated in this report. A wired monitoring system was used with uniaxial strain gauges spot welded to the members of the bridge. A data acquisition (DAQ) unit of type Spider8 from Hottinger Baldwin Messtechnik GmbH (HBM) together with a desktop computer were used for recording the data. The monitoring system could be managed and data files could be collected remotely through a mobile internet connection.

The strain gauges were located within the area indicated in Figure 5.2. The positions of the gauges are shown in Figure 5.3. Gauges 101 and 102 were mounted on the vertical flange edges of the stringer beam. Gauge 103 was mounted on the top of the flange close to the end of the cover plate. Gauge 104 was mounted to the bottom edge of the first diagonal of the main truss. Lastly, gauges 105 and 106 were mounted to the top of the crossbeam close to the edges. A more detailed drawing of the gauge positions can be found in Appendix I. All strain gauges were mounted with the purpose of measuring nominal strains without interference from local stress concentrations.

The photos in Figure 5.4(a) and Figure 5.4(b) shows the installed gauges 102 on the stringer beam and 105 on the crossbeam, respectively. The photos were taken before the gauges where covered with a weather protecting layer. The locker for the data acquisition system is shown in Figure 5.5.

5.2 Monitoring program

The monitoring started 25 October 2017 and was still ongoing at the time this report was written. The data evaluated in this report comprised passages until 30 April 2018. A total of 4 029 train passages were registered during this period.

A trigger level was used in the DAQ system to limit the registered data to train passages only. Each recorded train passage was saved in a separate file. A statistical evaluation based on the maximum stress range and the number of cycles has been performed to detect erroneous results. Outliers in the data were identified using the median absolute deviation (MAD). For a stochastic variable X it is calculated

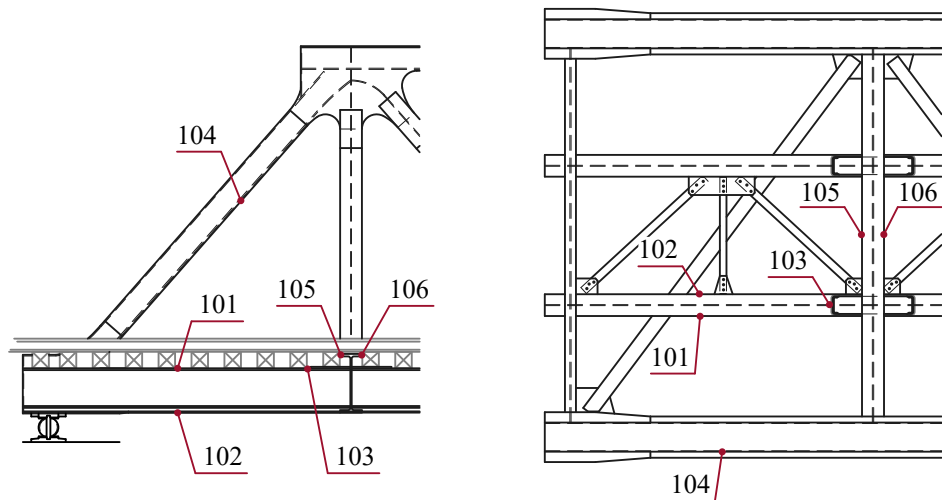


Figure 5.3: The locations of the strain gauges.



(a) Gauge 102.

(b) Gauge 105.

Figure 5.4: Photos of two installed strain gauges before the weather protection was applied.

as (Rousseuw and Croux, 1993)

$$MAD = \text{median}(|X_i - \text{median}(X)|) \quad (5.1)$$

for $i = 1, \dots, N$ samples. Outliers were identified as samples greater than six times MAD from the median. The factor six was selected based on a study on



Figure 5.5: The locker for the data acquisition (DAQ) system.

the robustness of the specific results from the Rautasjokk Bridge. A lower factor increases the risk of discarding real signals. The maximum stress ranges registered with gauge 101 for the train passages below the outlier threshold are shown in Figure 5.6. The threshold level for outliers is shown as a dashed line in the figure. The gaps in the data points, e.g. in the end of March and beginning of April, shows when the monitoring system unexpectedly shutted down.

All identified outliers were perfectly triangular or rectangular shaped strain peaks, typical for electrical disturbances. Out of the 4 029 train passages considered, only 149 were afflicted with disturbances. However, the stress peaks identified with the outlier threshold were distinct and could be discarded in the cycle counting which made it possible to also include these passages in the final evaluation.

5.3 Time history response

Examples on measured time histories are shown in Figure 5.7 for two different train passages. The first is due to a passage of an Intercity train with one locomotive and three wagons. The second shows the passage of an iron ore train composed by two locomotives and 68 heavy loaded wagons. The differences in load amplitude and number of cycles are apparent in the figure. Moreover, there is a fundamental

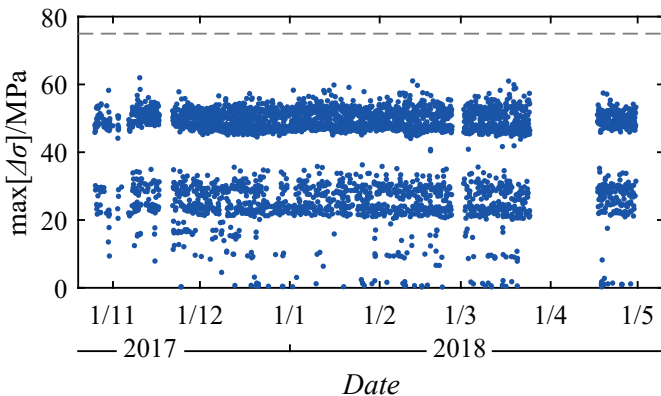


Figure 5.6: The maximum stress ranges for all train passages registered with gauge 101. The dashed line shows the threshold for the outliers.

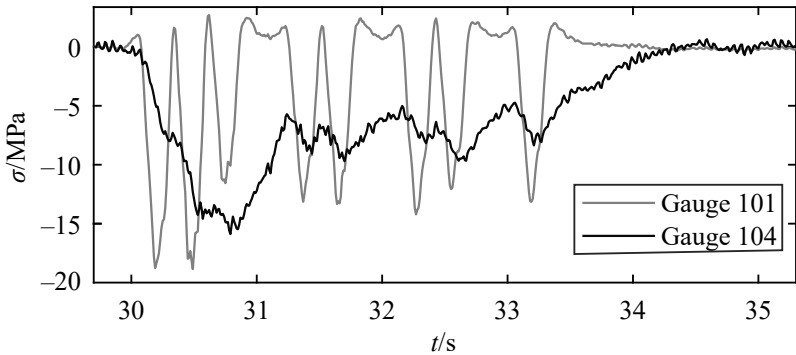
difference in the response between the two gauges. For gauge 101 located on the stringer beam, every bogie gives a distinct stress range. For gauge 104 on the main diagonal, the whole train produces one large cycle while the bogies cause minor variations.

The noise level in the measured response was relatively low. The strain measured when no train was on the bridge varied typically less than $\pm 2 \mu\text{m}/\text{m}$, corresponding to about $\pm 0.4 \text{ MPa}$. A histogram for 9 000 strain measurements for the unloaded bridge is shown in figure 5.8 valid for gauge 104. A fitted normal distribution is shown in the same figure and the rather good agreement implies that the noise follows a normal distribution.

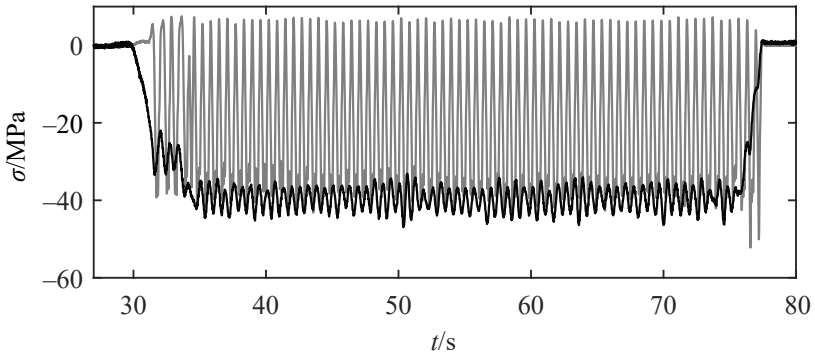
5.4 Stress range spectra

The stress range spectra for the measured response were derived in Matlab using the rainflow cycle counting technique as described in ASTM (2017). The spectra for all six strain gauges and the 4 029 registered passages are shown in Figure 5.9. A threshold at 9 MPa was considered in the presentation of the stress ranges.

An evaluation of the convergence rate of the measured response has been performed as suggested in Section 4.1, based on the equivalent stress range with the slope $m = 3$. The equivalent stress ranges over the number of passages are shown in Figure 5.10. The values are normalized with respect to the equivalent stress range after all 4 029 train passages. The results confirm the conclusion by Leander and



(a) Intercity train consisting of one locomotive and three waggons.



(b) Iron ore train consisting of two locomotives and 68 heavy loaded waggons.

Figure 5.7: Measured response for two different train passages and two different strain gauges.

Karoumi (2012) that the convergence rate can differ substantially between different gauge locations. A deviation of less than 5 % is reached after about 955 passages for gauge 104. For the other gauges, convergence is reached at a significantly fewer number of passages. With an assumption of 28 passing trains every day, a monitoring period of 34 days is required for gauge 104. The corresponding number for gauge 103 is 6 days.

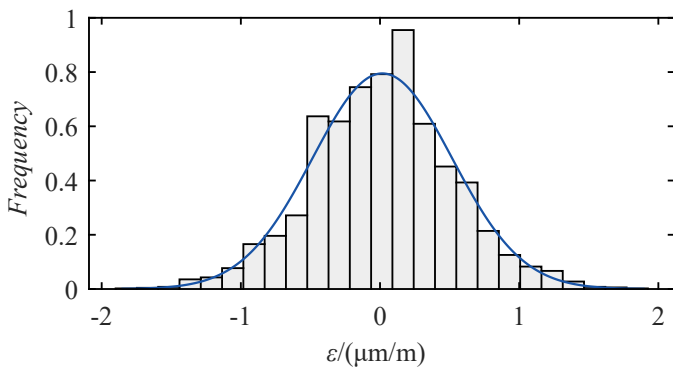


Figure 5.8: Distribution of strain measured with gauge 104 for the unloaded bridge. The continuous line shows a normal distribution fitted to the data.

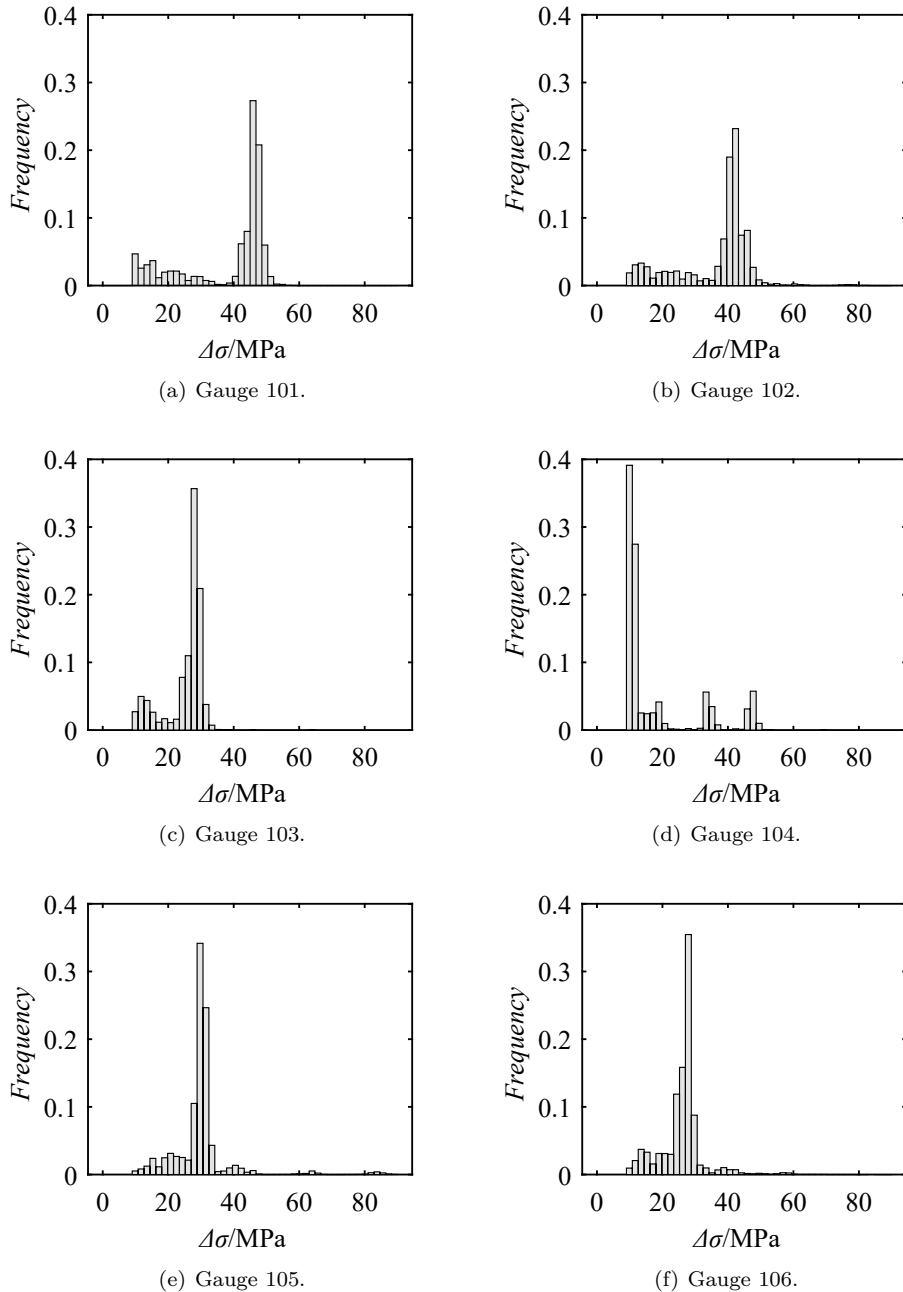


Figure 5.9: Normalized stress range spectra based on the measured response.

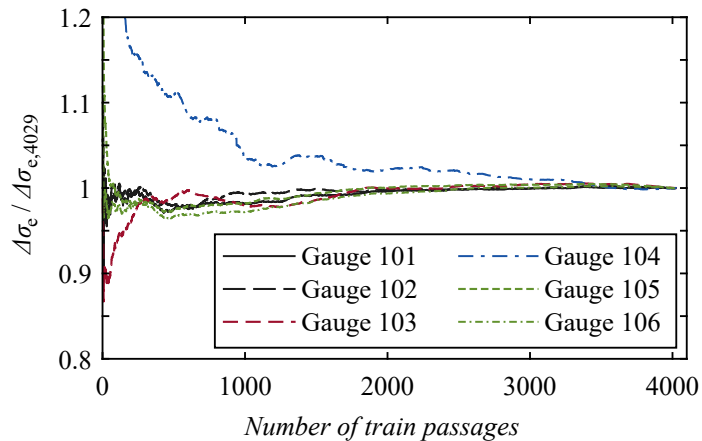


Figure 5.10: The equivalent stress ranges over the number of passages. The values are normalized with respect to the equivalent stress range after all 4 029 train passages.

5.5 Fatigue assessment

The fatigue assessments presented herein are superficial estimations of the remaining service life based on the methods presented in Chapter 2. The traffic volume was determined based on the measurements and was considered the same since the bridge opened in 1962. This causes an overestimation of the deterioration rate which should be kept in mind when interpreting the results. A more complete code based assessment can be found in the report by Häggström (2015).

Deterministic assessment

A deterministic fatigue assessment based on the measured response, the verification format defined by (2.3), and a bilinear S - N curve gave the result presented in Table 5.1. The assumed detail categories $\Delta\sigma_C$ were taken from EN 1993-1-9 and are stated in the same table. The partial safety factors were set to $\gamma_{MF} = 1.35$ and $\gamma_{Ff} = 1$. The fatigue lives were estimated based on an assumption of 28 train passages every day.

Table 5.1: The results of the deterministic fatigue assessment based on linear damage accumulation. The variable D_{mon} represent the accumulated damage for all registered train passages during the monitoring period.

Gauge	Location	$\Delta\sigma_C$ /MPa	D_{mon}	Fatigue life/years
101	Stringer	40	1.89×10^{-1}	2.1
102	Stringer	160	1.37×10^{-4}	>100
103	Stringer	50	1.97×10^{-2}	20
104	Main diagonal	100	1.49×10^{-4}	>100
105	Crossbeam	160	2.60×10^{-4}	>100
106	Crossbeam	160	3.46×10^{-5}	>100

The results of the deterministic assessment presented in Table 5.1 clearly show that the stringer beam is governing the fatigue life. The welded connection between the lateral bracing and the top flange of the beam attains the greatest accumulated damage and a fatigue life of merely 2 years. Also for the cover plate, a limited fatigue life as attained with a value of 20 years.

Probabilistic assessment

To reach a more elucidated picture of the fatigue deterioration of the detail at gauge 101, a probabilistic evaluation based on linear elastic fracture mechanics (LEFM) has been performed. The limit state equation defined by (2.12) was used together with a bilinear crack growth rate as described by Leander and Al-Emrani (2016). The stress intensity factor range $\Delta K(a)$ for this specific detail was calculated as

suggested by Leander et al. (2013). The characteristics of the detail are shown in Figure 5.11 and the properties of the basic variables in Table 5.2. The probability of failure was determined by Monte Carlo simulation.

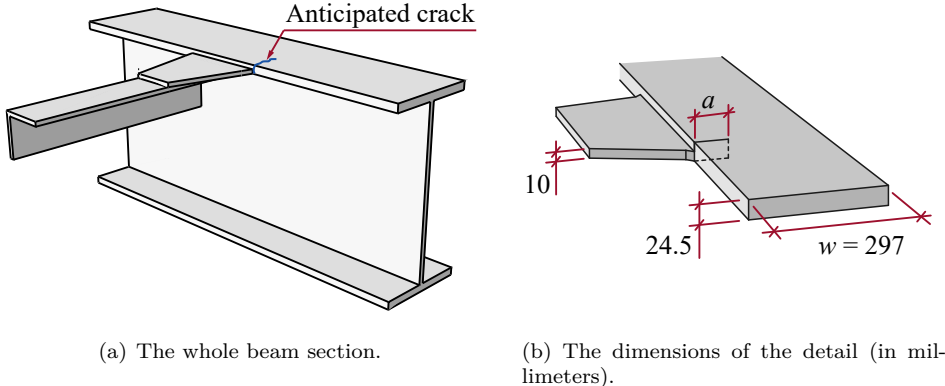


Figure 5.11: The stringer beam and the attachment of the lateral bracing.

Table 5.2: Basic variables variables. $N \sim \text{Normal}$, $\text{LN} \sim \text{Lognormal}$, $\text{DET} \sim \text{Deterministic}$. The values are valid for crack growth in mm/cycle and stress intensity in $\text{MPa}\sqrt{\text{mm}}$.

Variable	Distrib.	Mean	CoV
C_S	LN	1	0.03
C_{SIF}	LN	1	0.07
$\Delta\sigma$	DET		
A_a	LN	$4.80 \cdot 10^{-18}$	1.70
A_b	LN	$5.86 \cdot 10^{-13}$	0.60
m_a	DET	5.10	—
m_b	DET	2.88	—
K_{th}	LN	140	0.40
a_0	LN	0.15	0.66
a_c	DET	$w/2$	—

The results of the probabilistic assessment is shown in Figure 5.12 with the solid black line denominated prior, valid for the assessment without considering inspections. If the traffic intensity is assumed constant from 1962 until today, a target reliability of $\beta = 3.1$ was violated already after about three years (1965). This is in

line with the deterministic results presented in 5.1. At present time, the reliability is unreasonably low.

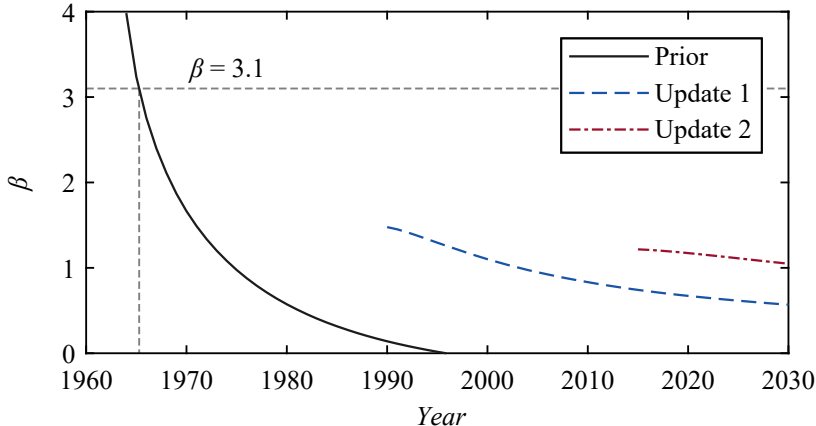


Figure 5.12: The reliability for the detail at gauge 101 estimated using LEFM. The results are based on the assumption that the traffic intensity has been constant and the same as during the measurements.

Reliability updating considering inspections

As described in Section 2.3, the reliability can be updated considering the outcome of inspections. According to the reports available in BaTMan, thorough examinations of the superstructure have been performed during the years 1990 and 2015 without any signs of cracks at the critical locations. Visual inspections are assumed and the variable a_d in (2.14) was modelled with a PoD curve described by (2.16) with $X_0 = 15.78$ and $b = 1.079$ valid for visual inspections and easy access to the examined detail (DNV GL, 2015). The PoD curve considered is shown in Figure 5.13. The rather low accuracy of the method is apparent in the figure. As an example, the probability of detecting a crack of size 20 mm is about 56 %. Nevertheless, considering the inspection outcome of a crude inspection method can still increase the predicted service life significantly.

The results of the reliability updating are shown as dashed lines in Figure 5.12. Both updates increases the reliability significantly. However, they do not provide enough information to raise the reliability above the target level of $\beta = 3.1$. A lower target level of $\beta = 2.3$ is supported by ISO 13822 (2010) if it is combined with recurrent inspections. But the estimated reliabilities are below this level also.

Despite the strong indications of fatigue damage, no cracks have been found during the inspections. The reason for this is most likely the conservative assumption in

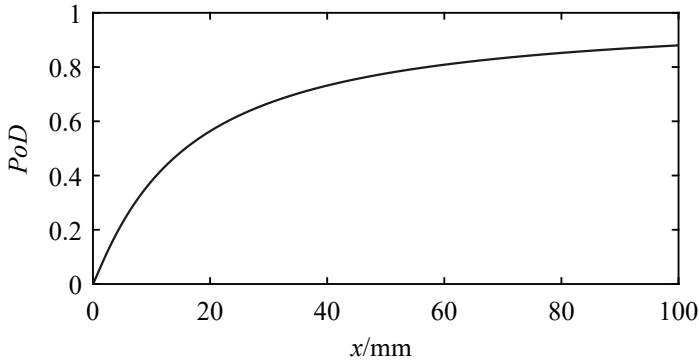


Figure 5.13: The probability of detection (PoD) for visual inspections and easy access to the examined detail. The x-axis represents the visual length of the crack.

the theoretical assessment that the whole stress range is crack driving even though a part of it acts in far field compression. This assumption stems from tests showing that residual stresses from the welding process can have a significant influence on the local stresses close to the weld (Sonsino, 2009). Without detailed knowledge about the residual stress field, the analyst must make a conservative assumption that the whole stress history can be shifted into tensile stress, see e.g., paragraph 8.2.1.4 in BSI (2013).

5.6 Summary

The monitoring campaign of the Rautasjokk Bridge comprise 6 strain gauges at the positions indicated in Figure 5.3. A more detailed description of the positions can be found in the Appendix I.

A fatigue assessment based on the measured response confirms the strongly limited fatigue life reached in previous assessments. An assessment based on probabilistic fracture mechanics and a reliability updating based on inspections allows an increase in the reliability but still an insufficient service life, see Figure 5.12.

Chapter 6

Results of response predictions

This chapter presents some results from tests of the prediction methods described in Chapters 3 and 4. The calculations were based on the measured data from the Rautasjokk Bridge.

For fitting and training of the prediction models, theoretical response calculations were performed using influence lines from the FE model developed by Lundman and Parnéus (2018). Figure 6.1 shows the two influence lines for the gauge locations 101 and 104 located on the stringer beam and the main diagonal, respectively, see Figure 5.3 for the locations of the gauges.

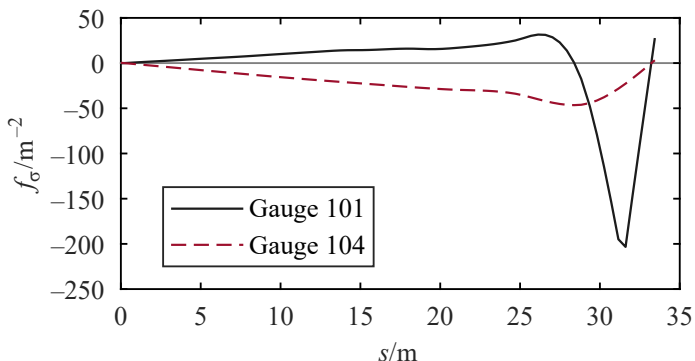


Figure 6.1: Influence lines for the stresses at the gauge locations 101 and 104 for different positions s along the bridge.

The influence lines were loaded with real train configurations from traffic measurements performed by the company Damill AB at Tornehamn, about 90 km northwest of the bridge location. Descriptions of 33 train passages registered Wednesday 14

February 2018 were provided comprising a mixture of iron ore trains and Intercity trains. The shortest and longest trains had 16 and 284 axles, respectively.

6.1 Time history prediction

An ANN as described in Section 3.3 was trained using time histories calculated with the theoretical influence lines and all 33 train passages. The response at position 101 and 104 was used as input and target, respectively. An evaluation of the performance of the trained network was based on the root mean squared error (RMSE) for the theoretical and predicted response of a selected train passage. The design of the network was adjusted to minimize the RMSE. The final network consisted of 37 input neurons, two hidden layers with 30 neurons in each, and one output neuron. In Figure 6.2, the predicted response using the trained network is shown when the input is based on the theoretical evaluation of the influence lines, viz. the same model as used for training. The figure shows a very high level of agreement between the predicted and target responses.

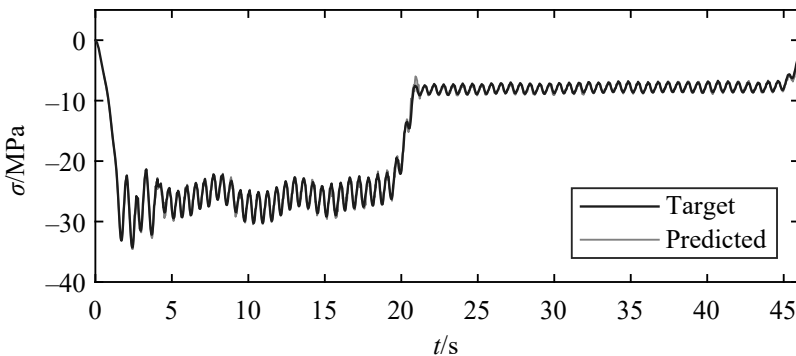


Figure 6.2: Predicted response from the passage of a train based on input from the theoretical evaluation of the influence lines.

The trained network was then used for predicting the response at position 104 using response measured with gauge 101 as input. The predicted response for the passage of a train is shown in Figure 6.3. Large differences are apparent in the figure showing that the trained network does not provide trustworthy predictions when the input is measured stress. Apparently, there are too large differences in the input from the theoretical model and from the measurements.

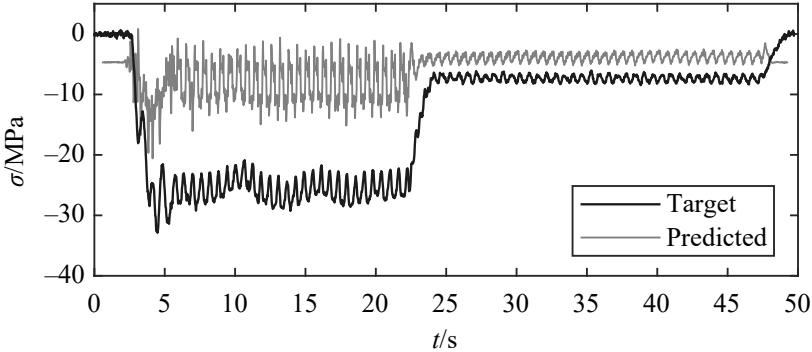


Figure 6.3: Predicted response from the passage of a train based on measured input.

6.2 Stress range spectra predictions

Multivariate linear regression

Predictions of the response in terms of stress range spectra have been performed using multivariate linear regression as described in Section 4.2. Theoretically calculated stress range spectra for the 33 individual train passages, the same as used in the time history prediction, were used for fitting the coefficient matrix. The spectra for gauges 101 and 104 were assigned predictor and response, respectively. The fitted coefficient matrix was then used as a transformation matrix to predict a new spectrum at gauge location 104 using measured response at location 101. Figure 6.4(a) shows the predicted and target spectra for the passage of a single train, the same passage as shown as a time history in Figure 6.3. There is an obvious difference in the distribution of the stress ranges but the equivalent stress ranges are fairly close, 12.6 MPa and 13.9 MPa for the predicted and target spectra, respectively.

The predicted spectrum for the whole monitoring period is shown in Figure 6.4(b). As for the single train passage, the difference in stress range distribution is obvious even though the stress ranges are allocated in the same regions. The equivalent stress ranges for the predicted and target spectra are 13.9 MPa and 13.2 MPa, respectively.

Neural network fitting

As an alternative to the linear regression, a nonlinear fitting was performed using an ANN as described in Section 4.3. The training input to the ANN consisted of the stress range spectra for the 33 train passages. The number of cycles for stress ranges in the span 5 MPa to 91 MPa were considered, however, stress ranges with

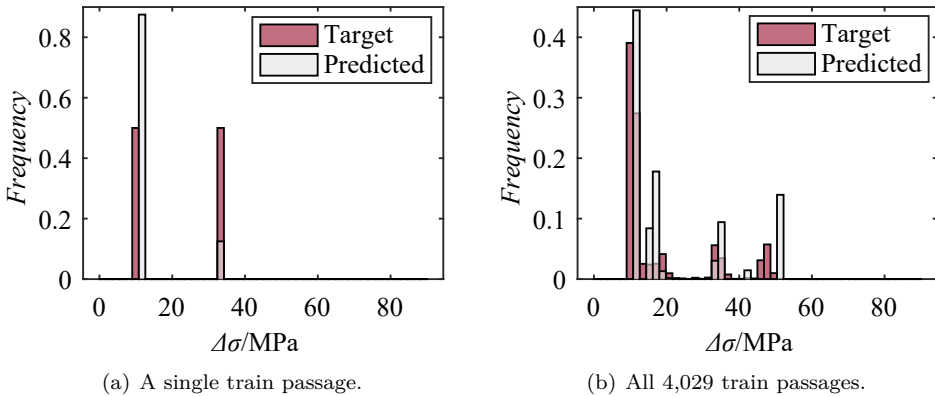


Figure 6.4: Predicted stress range spectra based on measured input using multi-variate linear regression.

zero cycles were omitted which gave a total of 77 considered stress ranges. The number of neurons in the input and output layers were the same as the considered stress ranges. One hidden layer with 30 neurons was modelled.

One of the best predictions for a single train passage is shown in Figure 6.5(a). Still, differences in the distributions of the stress ranges are apparent. The equivalent stress ranges are 10.0 MPa and 13.9 MPa for the predicted and target spectra, respectively.

The predicted spectrum for the whole monitoring period is shown in Figure 6.5(b). The equivalent stress ranges are 15.0 MPa and 13.9 MPa for the predicted and target spectra, respectively.

It should be noted that the predictions using an ANN are not stable for this setting. The spectra varies substantially between network designs and individual runs. One reason may be the limited training set of merely 33 theoretical train passages.

6.3 Summary

For time history prediction, a high accuracy is possible with an artificial neural network (ANN), when the prediction is based on input from the same theoretical model as used for training. Deceptive predictions were attained when the trained network was fed with input from measurements. An example is shown in Figure 6.3 showing large differences between the predicted and target responses.

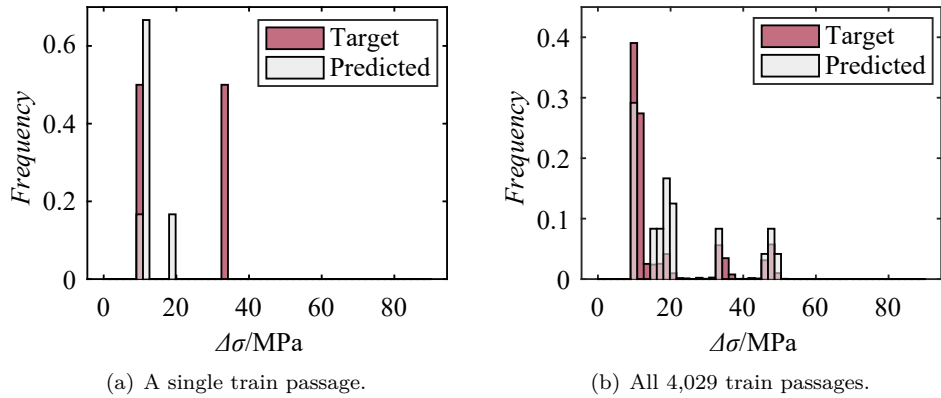


Figure 6.5: Predicted stress range spectra based on measured input using a fitted ANN.

For predictions based on stress range spectra, multivariate linear regression produced reasonable accuracy in terms of equivalent stress range. For the whole monitoring period, the deviation from the true equivalent stress range based on measurements was about 6 %.

A neural network fitting based on stress range spectra did not produce trustworthy predictions for the setting presented. Significant differences in equivalent stress range spectra were attained. Furthermore, the results were not consistent between runs.

Chapter 7

Discussion and conclusions

The review of methods for response prediction is in no sense exhaustive. The fields of *state observers* in control theory , *machine learning* in computer science, and *autoregressive models* for system identification are extensive and covers a broad variation of applications. The selection of methods was made under the condition that they should be applicable for response prediction at unmeasured locations. The assumption that the true response at the unmeasured location remains unknown during measurements means that no feedback information will be available. Furthermore, the time-variant relation between the response at different locations in a structure entangles linear methods.

The possibility to fit/train a model using theoretically calculated response and then perform predictions based on measured response has been investigated. This has appeared difficult during the work. Signals with even small deviations from the training data have rendered incorrect predictions. This makes it dubious to fit/train a model based on theoretical response and then use it for predictions based on measured input, without any feedback from the unmeasured location.

The design and training of the artificial neural networks have shown to be crucial for the predictions. This is emphasized also by Zhang (2012). In the current study, where the true measured response was available, the number of layers and neurons could be varied to improve the accuracy. This is, however, not possible in predictions at unmeasured locations in real cases, making it difficult to trust the predictions for assessment.

7.1 Conclusions

The conclusions are based on the evaluation of a few selected methods for response prediction at unmeasured locations using a small scale monitoring system.

- For bridge details prone to fatigue, the stress history is dominated by a quasi-static response due to vehicle passages. Furthermore, the relation between different locations is time-variant. These conditions complicate the use of established linear methods for response prediction as, e.g., Kalman filtering.
- For time history prediction, artificial neural networks constitutes a powerful tool capable of delivering a high accuracy – if the input agrees with the training set. For even small deviations, questionable predictions were reached.
- Multivariate linear regression appears promising for response prediction based on stress range spectra. A deviation of merely 6 % for the equivalent stress range was attained for a specific example from the Rautasjokk Bridge.
- The use of an artificial neural network (ANN) for predictions based on stress range spectra was not successful for the setting in this investigation. With a small training set of 33 train passages the ANN did not provide trustworthy predictions.

Regarding the Rautasjokk Bridge and the monitoring between October 2017 and April 2018, the following conclusions can be drawn.

- The monitoring system has provided high quality measurements of 4 029 train passages during the considered period. The noise level is typically less than $\pm 2 \mu\text{m}/\text{m}$.
- The convergence rate for the stress range spectra differs between gauge locations from a couple of days to a maximum of 34 days.
- A fatigue assessment based on the measured response confirms the strongly limited fatigue life reached in previous assessments.
- An assessment based on probabilistic fracture mechanics and a reliability updating based on inspections allows an increase in the reliability but still an insufficient service life.

7.2 Future research

The superficial review of possible methods for response prediction should be extended. The methods treated in this report are a limited first selection. The review should also include the aspect of connecting different measured quantities as, e.g., accelerations and strains to reach an accurate prediction.

If artificial neural networks are to be used, an in-depth treatment of the design of the network will be required including a theoretical study on available training (learning) techniques.

Bibliography

- Amzallag, C., Gerey, J. P., Robert, J. L., Bahuaud, J., 1994. Standardization of the rainflow counting method for fatigue analysis. *International Journal of Fatigue* 16 (4), 287–293.
- ASTM, 2017. Standard Practices for Cycle Counting in Fatigue Analysis. ASTM International, West Conshohocken, PA, E1049-85(2017).
- BSI, 2013. Guide to methods for assessing the acceptability of flaws in metallic structures. The British Standards Institution (BSI), BS 7910:2013.
- CEN, 2006. Eurokod 3: Dimensionering av stålkonstruktioner – Del 1-9: Utmatting. European committee for standardization (CEN), SS-EN 1993-1-9.
- CEN, 2009. Eurokod 3: Dimensionering av stålkonstruktioner – Del 2: Broar. European committee for standardization (CEN), SS-EN 1993-2.
- CEN, 2010. Eurokod – Grundläggande dimensioneringsregler för bärverk. European committee for standardization (CEN), SS-EN 1990.
- Chatzi, E. N., Smyth, A. W., 2015. Nonlinear system identification: Particle-based methods. In: Beer, M., Kougioumtzoglou, I. A., Patelli, E., Au, S.-K. (Eds.), *Encyclopedia of Earthquake Engineering*. Springer Berlin Heidelberg, Berlin, Heidelberg, pp. 1677–1692.
- Connor, R. J., Fisher, J. W., 2006. Identifying effective and ineffective retrofits for distortion fatigue cracking in steel bridges using field instrumentation. *Journal of Bridge Engineering* 11 (6), 745–752.
- Dexter, R. J., Wright, W. J., Fisher, J. W., 2004. Fatigue and fracture of steel girders. *Journal of Bridge Engineering* 9 (3), 278–286.
- DNV GL, 2015. Probabilistic methods for planning of inspection for fatigue cracks in offshore structures. DNV GL AS, DNVGL-RP-C210.
- Grewal, M. S., Andrews, A. P., 2015. Kalman filtering – Theory and practice using MATLAB. John Wiley & Sons, Inc.

- Hagan, M. T., Demuth, H. B., Beale, M. H., De Jesús, O., 2014. Neural network design. Marting Hagan.
- Hagan, M. T., Menhaj, M. B., 1994. Training feedforward networks with the marquardt algorithm. *IEEE Transactions on Neural Networks* 5 (6), 989–993.
- Hajializadeh, D., OBrien, E. J., O'Connor, A. J., 2017. Virtual structural health monitoring and remaining life prediction of steel bridges. *Canadian Journal of Civil Engineering* 44 (4), 264–273.
- Haykin, S., 2009. Neural Networks and Learning Machines. Pearson Education, Inc.
- Häggström, J., 2015. Bärighetsberäkning: Bro över Rautasjökk km 1432+883 (in Swedish). Report, Luleå University of Technology.
- Häggström, J., Blanksvärd, T., Collin, P., 2016. Fatigue assessment of stringer beams using structural health monitoring. In: Elfgrén, L., Jonsson, J., Karlsson, M., Rydberg-Forssbeck, L., Sigfrid, B. (Eds.), 19th IABSE Congress Stockholm: Challenges in Design and Construction of an Innovative and Sustainable Built Environment. pp. 1450–1457.
- Hobbacher, A. F., 1992. Stress intensity factors of plates under tensile load with welded-on flat side gussets. *Engineering Fracture Mechanics* 41 (6).
- Hobbacher, A. F., 2016. Recommendations for fatigue design of welded joints and components. Springer International Publishing.
- Iliopoulos, A., Weijtjens, W., Van Hemelrijck, D., Devriendt, C., 2017. Fatigue assessment of offshore wind turbines on monopile foundations using multi-band modal expansion. *Wind Energy* 20 (8), 1463–1479.
- ISO 13822, 2010. Bases for design of structures – Assessment of existing structures. International Organization for Standardization (ISO).
- Jarfäll, L., 1974. Livslängdsberäkning-kumulativ skadeverkan vid utmattning. Väg- och vattenbyggaren (10).
- JCSS, 2011. Probabilistic model code - Part 3: Resistance models. Joint Committee on Structural Safety (JCSS).
- Kalman, R. E., 1960. On the general theory of control systems. In: Proceedings of the first international congress of IFAC.
- Kühn, B., Lukic, M., Nussbaumer, A., Günther, H., Helmerich, R., Herion, S., Kolstein, M., Walbridge, S., Androic, B., Dijkstra, O., Bucak, O., 2008. Assessment of Existing Steel Structures: Recommendations for Estimation of Remaining Fatigue Life. Prepared under the JRC-ECCS cooperation agreement for the evolution of Eurocode 3.

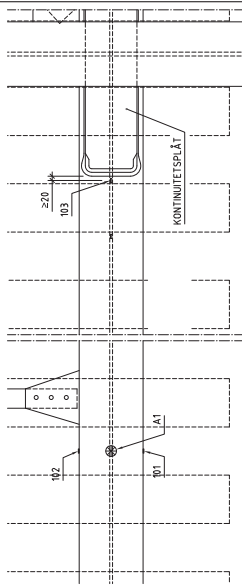
- Leander, J., Al-Emrani, M., 2016. Reliability-based fatigue assessment of steel bridges using lefm – a sensitivity analysis. *International Journal of Fatigue* 93 (1), 82–91.
- Leander, J., Andersson, A., Karoumi, R., 2010. Monitoring and enhanced fatigue evaluation of a steel railway bridge. *Engineering Structures* 32 (3).
- Leander, J., Aygül, M., Norlin, B., 2013. Refined fatigue assessment of joints with welded in-plane attachments by lefm. *International Journal of Fatigue* 56, 25–32.
- Leander, J., Honfi, D., Larsson Ivanov, O., Björnsson, I., 2018. A decision support framework for fatigue assessment of steel bridges, accepted for publication.
- Leander, J., Karoumi, R., 2012. Quality assurance of measured response intended for fatigue life prediction. *Journal of Bridge Engineering* 17 (4), 711–719.
- Leander, J., Norlin, B., Karoumi, R., 2015. Reliability-based calibration of fatigue safety factors for existing steel bridges. *Journal of Bridge Engineering* 20 (10).
- Liu, M., Frangopol, D. M., Kwong, K., 2010. Fatigue reliability assessment of retrofitted steel bridges integrating monitored data. *Structural Safety* 32 (1).
- Lundman, S., Parnéus, P., 2018. Virtual sensing for fatigue assessment of the Rautasjökk Bridge. Master thesis TRITA-ABE-MBT-18193, KTH Royal Institute of Technology.
- Maddox, S. J., 1991. Fatigue strength of welded structures. Woodhead Publishing.
- Madsen, H. O., Krenk, S., Lind, N. C., 2006. Methods of structural safety. Dover Publications Inc., New York.
- Maes, K., Iliopoulos, A., Weijtjens, W., Devriendt, C., Lombaert, G., 2016. Dynamic strain estimation for fatigue assessment of an offshore monopile wind turbine using filtering and modal expansion algorithms. *Mechanical Systems and Signal Processing* 76–77, 592–611.
- Miner, M. A., 1945. Cumulative damage in fatigue. *Journal of Applied Mechanics* 67, A159–A164.
- Ogata, K., 2010. Modern control engineering. Prentice Hall, Upper Saddle River, N.J.
- Olive, D. J., 2017. Linear Regression. Springer International Publishing AG.
- Pai, S. G. S., Nussbaumer, A., Smith, I. F. C., 2018. Comparing structural identification methodologies for fatigue life prediction of a highway bridge. *Frontiers in Built Environment* 3, 73.

- Palanisamy, R. P., Cho, S., Kim, H., Sim, S.-H., 2015. Experimental validation of kalman filter-based strain estimation in structures subjected to non-zero mean input. *Smart Structures and Systems* 15 (2), 489–503.
- Palmgren, A., apr 1924. Die Lebensdauer von Kugellagern. *VDI Zeitschrift* 68 (14).
- Papadimitriou, C., Fritzen, C.-P., Kraemer, P., Ntotsios, E., 2011. Fatigue predictions in entire body of metallic structures from a limited number of vibration sensors using kalman filtering. *Structural Control and Health Monitoring* 18 (5), 554–573.
- Paris, P. C., Gomez, M. P., E., A. W., 1961. A rational analytic theory of fatigue. *The Trend in Engineering* 13 (1).
- Rousseeuw, P. J., Croux, C., 1993. Alternatives to the median absolute deviation. *Journal of the American Statistical Association* 88 (424), 1273–1283.
- Schilling, C. G., Klippstein, K. H., 1977. Fatigue of steel beams by simulated bridge traffic. *Journal of the Structural Division – ASCE* 103 (ST8), 1561–1575.
- Sonsino, C., jan 2009. Effect of residual stresses on the fatigue behaviour of welded joints depending on loading conditions and weld geometry. *International Journal of Fatigue* 31 (1).
- Stephens, R. I., Fatemi, A., Stephens, R. R., Fuchs, H. O., 2001. Metal fatigue in engineering. John Wiley & Sons, Inc.
- Straub, D., 2014. Value of information analysis with structural reliability methods. *Structural Safety* 49, 75–85.
- Straub, D., Chatzi, E., Bismut, E., Courage, W. M. G., Döhler, M., Faber, M. H., Köhler, J., Lombaert, G., Omenzetter, P., Pozzi, M., Thöns, S., Val, D., Wenzel, H., Zonta, D., 2017. Value of information: A roadmap to quantifying the benefit of structural health monitoring. In: Bucher, C., Ellingwood, B. R., Frangopol, D. M. (Eds.), 12th Int. Conf. on Structural Safety and Reliability (ICOSSAR). pp. 3018–3029.
- Suresh, S., 1998. Fatigue of materials. Cambridge University Press.
- Sustainable Bridges, 2007. Monitoring guidelines for railway bridges. Sustainable Bridges – Assessment for Future Traffic Demands and Longer Lives, Deliverable D5.2.
- Trafikverket, 2004. BaTMan – Bridge and tunnel management. Swedish Transport Administration (Trafikverket), <https://batman.trafikverket.se>.
- Trafikverket, 2017. Bärighetsberäkning av broar (in Swedish). Swedish Transport Administration (Trafikverket), TDOK 2013:0267, version 4.0.

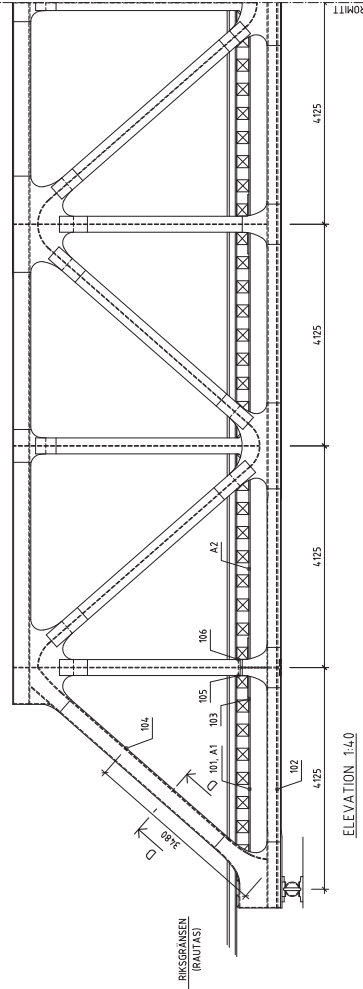
- Wong, K.-Y., 2007. Design of a structural health monitoring system for long-span bridges. *Structure and Infrastructure Engineering* 3 (2), 169–185.
- Zhang, G. P., 2012. Neural networks for time-series forecasting. In: Rozenberg, G., Bäck, T., Kok, J. N. (Eds.), *Handbook of Natural Computing*. Springer Berlin Heidelberg, Berlin, Heidelberg, pp. 461–477.
- Zhou, Y. E., 2006. Assessment of bridge remaining fatigue life through field strain measurement. *Journal of Bridge Engineering* 11 (6), 737–744.

Appendix I

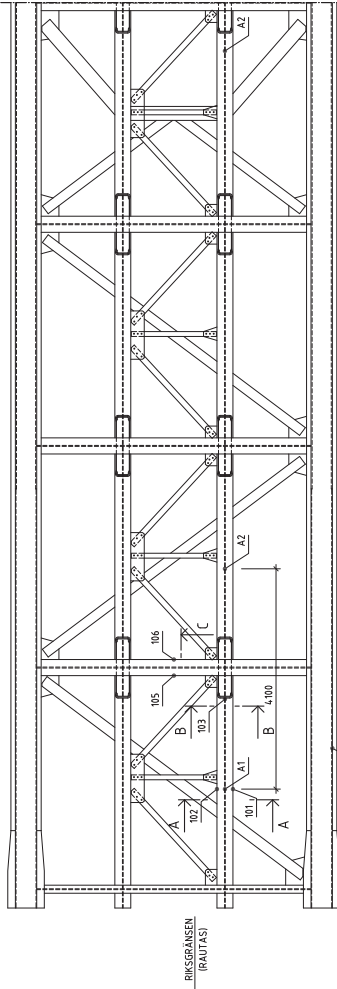
Instrumentation drawing



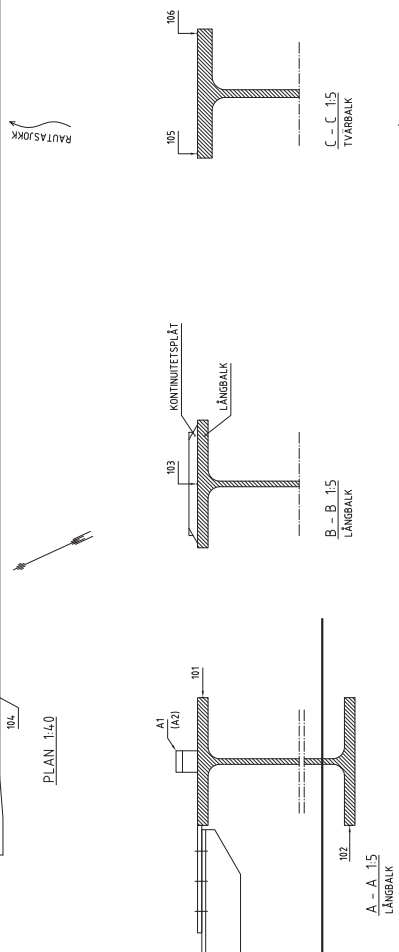
DELPLANER 1:10
GIVARE PÅ LÄNGBALK



ELEVATION 1:40



PLAN 1:40



$$\frac{A - A_{15}}{B - B_{15}} = \text{LANGKAL}$$

C - C 1:5

KIRUNA
(KROKVIK)

D - D 1:5
DIAGONALSTÅNG

KTH